

# Cross Algorithms for Cost-Effective Time Integration of Nonlinear Tensor Differential Equations on Low-Rank Tucker Tensor and Tensor Train Manifolds

Behzad Ghahremani<sup>1</sup> and Hessam Babaei<sup>1\*</sup>

*Department of Mechanical Engineering and Materials Science, University of Pittsburgh, 3700 O'Hara Street, Pittsburgh, PA, 15213, USA*

*\* Corresponding Author, Email:h.babaei@pitt.edu*

---

## Abstract

Dynamical low-rank approximation (DLRA) provides a rigorous, cost-effective mathematical framework for solving high-dimensional tensor differential equations (TDEs) on low-rank tensor manifolds. Despite their effectiveness, DLRA-based low-rank approximations lose their computational efficiency when applied to nonlinear TDEs, particularly those exhibiting non-polynomial nonlinearity. In this paper, we present a novel algorithm for the time integration of TDEs on the tensor train and Tucker tensor low-rank manifolds, which are the building blocks of many tensor network decompositions. This paper builds on our previous work (*Donello et al., Proceedings of the Royal Society A, Vol. 479, 2023* [1]) on solving nonlinear matrix differential equations on low-rank matrix manifolds using CUR decompositions. The methodology we present offers multiple advantages: (i) it leverages cross algorithms based on the discrete empirical interpolation method to strategically sample sparse entries of the time-discrete TDEs to advance the solution in low-rank form. As a result, it offers near-optimal computational savings both in terms of memory and floating-point operations. (ii) The time integration is robust in the presence of small or zero singular values. (iii) The algorithm is remarkably easy to implement, as it requires the evaluation of the full-order model TDE at strategically selected entries and it does not use tangent space projections, whose efficient implementation is intrusive and time-consuming. (iv) We develop high-order explicit Runge-Kutta schemes for the time integration of TDEs on low-rank manifolds. We demonstrate the efficiency of the presented algorithm for several test cases, including a 100-dimensional TDE with non-polynomial nonlinearity.

**Keywords:** Tensor train decomposition, Tucker tensor decomposition, dynamical low-rank approximation, time-dependent bases, cross approximation

---

## 1. Introduction

Multi-dimensional tensors are of significant importance in many scientific and engineering applications [2]. For a  $d$ -dimensional tensor of size  $n_1 \times n_2 \times \dots \times n_d$ , the computational cost or memory requirement scales with  $\mathcal{O}(n^d)$ , where  $n = n_i$ ,  $i = 1, \dots, d$ . This exponential relation between the number of tensor elements and the dimension ( $d$ ) is known as the curse of dimensionality. Tensor low-rank approximation methods have been developed to tackle this issue by utilizing the advantage of multi-dimensional correlations [3]. Leveraging low-rank approximation methods enables a potentially significant reduction in the total number of tensor elements, with the ability to control the accuracy loss by varying the rank. Tucker tensor decomposition [4], CANDECOMP/PARAFAC

(CP) [5], hierarchical Tucker tensor decomposition [6], and tensor train decomposition/matrix product states [7, 8] are well-known tensor low-rank approximation approaches. Tensor train decomposition, in particular, reduces the number of elements of a given tensor from  $n^d$  to  $dnr^2$ , where  $r$  is the maximal tensor train rank. Accordingly, tensor train decomposition effectively eliminates the exponential dependence on  $d$  [9]. Example applications of tensor train decomposition in various fields include system identification [10], electronic design automation [11], large-scale matrix processing [12], machine learning [13, 14], and data mining [15]. The Tucker tensor low-rank approximation reduces the total number of elements of a  $d$ -dimensional tensor from  $n^d$  to  $r^d + rdn$ , where  $r$  represents the rank of the unfolded tensors along each mode. The Tucker tensor and tensor train trees are the building blocks for many tensor network approximations [16]. These two tensor low-rank approximations are the focus of this study.

One important application of tensor train and Tucker decomposition is the reduction of computational costs in solving multi-dimensional partial differential equations (PDEs) through dynamical low-rank approximation (DLRA) [17, 18]. Discretizing time-dependent, multi-dimensional PDEs in all dimensions except time results in tensor differential equations (TDEs) in the form  $dV/dt = \mathcal{F}(V)$ , where  $V \in \mathbb{R}^{n_1 \times n_2 \times \dots \times n_d}$  is the solution tensor, and  $\mathcal{F}(V)$  is the right-hand side tensor of the same size as  $V$ . For applications of DLRA in solving the Schrödinger equation and Hamilton-Jacobi-Bellman equations, see [19, 20]. The tensor train/MPS low-rank approximation has recently been used to perform direct numerical simulation of turbulent flows [21]. Solving these TDEs, even in moderate dimensions (e.g.,  $d = 4, 5, 6$ ), using traditional numerical methods such as finite difference and finite element methods, encounters the issue of the curse of dimensionality [22]. To decrease the number of degrees of freedom of  $V(t)$ , DLRA constrains the solution of the TDEs to the manifold of low-rank tensors, where explicit evolution equations are obtained in the compressed, low-rank tensor train and Tucker formats.

Despite the effectiveness of DLRA in reducing the computational cost of solving multi-dimensional TDEs, several challenges remain as enumerated below:

1. **Computational Cost:** The computational cost of solving DLRA increases when the exact rank of  $\mathcal{F}(V)$  is high. This issue arises in linear TDEs featuring a large number of right-hand side terms or full-rank forcing matrices [23, 24] and in TDEs with high-order polynomial nonlinearities. For TDEs that incorporate non-polynomial nonlinearities, such as exponential or fractional nonlinearity, the floating-point operation (flop) costs of solving the DLRA evolution equations exceed those of the full-order model (FOM). This increase in cost is due to the fact that  $\mathcal{F}(V)$  becomes a full-rank tensor even when  $V$  is of low rank. Consequently,  $\mathcal{F}(V)$  needs to be formed explicitly, requiring  $\mathcal{O}(n^d)$  flop costs, which are similar to those of the FOM. While the DLRA equations can still be solved in a memory-efficient manner by sequentially computing entries of  $\mathcal{F}(V)$ , this approach results in increased wall clock time due to the sequential nature of the algorithm.
2. **Intrusiveness:** Even when the exact rank of  $\mathcal{F}(V)$  is low, for example, for linear TDEs, the efficient implementation of DLRA evolution equations is intrusive, for example, when dealing with complex codes, such as multi-physics problems. This process involves substituting the low-rank approximation in the FOM, and projection of  $\mathcal{F}(V)$  onto the tangent space of the manifold [1, 25]. However, to retain the memory and flops efficiencies that the DLRA offers, the implementation must be done carefully to avoid forming tensors in the ambient space or forming tensors that require significantly more degrees of freedom than what is needed to

represent  $V$  on the low-rank manifold.

3. **Ill-Conditioning:** The DLRA evolution equations obtained from the projection onto the tangent space of the manifold may encounter numerical stability issues. The computation of the evolution equations involves inverting auto-correlation matrices that may become ill-conditioned as time integration proceeds [18, 26–28]. This is especially problematic when the rank ( $r$ ) of the system is increased to achieve a more accurate approximation. The inversion of these possibly ill-conditioned matrices causes stringent constraints on time step size in numerical integration and error amplification. In dynamical tensor train approximation, small singular values of unfolded core tensors are the source of ill-conditioning.

The aforementioned issues have been the focus of intense research in the past decade. Projector-splitting techniques [26, 29] utilize a Lie–Trotter or Strang splitting of the tangent-space projection. These time integration schemes are robust in the presence of small or zero singular values, however, they involve a backward time step, which renders these techniques unstable for dissipative dynamical systems. The robust basis update & Galerkin (BUG) integrators [28, 30, 31] are robust in the presence of small or zero singular values and are stable for dissipative dynamical systems. These techniques have also been extended to tensor networks [32, 33]. However, these techniques have a first-order temporal accuracy. Recently, a second-order robust BUG integrator based on the midpoint rule was introduced [34]. In [35], a projection method was introduced, in which higher-order Runge-Kutta schemes are applied to the projected equation. In [36], a similar approach was presented, which is based on the rank-truncation of the time-discrete evolution equations and can achieve high-order temporal accuracy.

The focus of the above studies has been on developing stable time integration schemes. However, the issue of the computational cost is not addressed for nonlinear MDEs/TDEs. The issue of computational cost was first addressed in [25], in the context of DLRA for MDEs, where a low-rank approximation of  $\mathcal{F}(V)$  is constructed using an interpolatory CUR decomposition. The approach presented [25] requires evaluating  $\mathcal{F}(V)$  at  $r$  columns and rows. The columns and rows are selected based on the Discrete Empirical Interpolation Method (DEIM) [37]. Therefore, this approach evaluates  $\mathcal{F}(V)$  at  $r(n_1 + n_2)$  entries, which are the minimum number of entries required to build a rank- $r$  approximation of  $\mathcal{F}(V)$  of size  $n_1 \times n_2$ . A similar technique has also been introduced in [38] for hyper-reduction of parametric Hamiltonian dynamical systems. We recently extended this approach to DLRA of TDEs in the Tucker tensor form [39]. For an overview of the DEIM algorithm for nonlinear reduced order modeling, we refer the reader to [39]. At the time of preparation of this manuscript a similar interpolatory low-rank approximation [40] was proposed for tensor train integration which interpolates  $\mathcal{F}(V)$  onto the tangent space. All of these techniques are based on DLRA and tangent space projections.

Recently, we introduced an algorithm [1] for the time integration of nonlinear MDEs on low-rank manifolds. The algorithm presented in [1] does not utilize tangent space projection. The algorithm applies CUR interpolatory low-rank approximation to the time-discrete MDE. The algorithm presented in [1] is cost-optimal regardless of the type of nonlinearity of  $\mathcal{F}(V)$ , i.e., at each time instant it only evaluates  $r(n_1 + n_2)$  entries of the time-discrete MDE. Moreover, the algorithm does not utilize inversion of singular values and it is robust in the presence of small or zero singular values and it can achieve high-order temporal accuracy.

In this paper, we introduce a novel algorithm for the time integration of TDEs on low-rank manifolds, addressing the aforementioned challenges. In particular, we build on our previous work

[1] and develop new time integration schemes for TDEs in Tucker tensor and tensor train forms. The combination of these forms can generate both binary and non-binary tensor tree networks, therefore showcasing the potential applicability of the developed techniques to complex tensor networks. The schematic of the presented algorithm is shown in Figure 1. The contributions of this paper are listed as follows:

- We present **TT-CUR-DEIM (iterative)**, a new tensor train-cross algorithm in which fibers are selected based on DEIM [37]. The algorithm is very similar to the TT-CROSS-maxvol algorithm from [8] with the difference that the maxvol algorithm is replaced with DEIM. The DEIM algorithm requires access to exact or approximate singular vectors, which are not available in many applications. Unlike DEIM, the **TT-CUR-DEIM (iterative)** algorithm does not require access to the singular vectors and can be used as a *black box* tensor train cross algorithm. If exact or approximate singular vectors are available, no iterations are required. In such cases, we refer to the algorithm simply as **TT-CUR-DEIM**. The proposed algorithm complements the recently proposed **DEIM-FS (iterative)** algorithm [39], which is a black box Tucker tensor cross algorithm based on DEIM fiber sampling (FS).
- We propose a *unified* time integration approach for solving TDEs on low-rank Tucker tensor and tensor train manifolds, which effectively address the challenges highlighted above. (i) For the tensor train decomposition, the computational complexity of our proposed methodology scales with  $\mathcal{O}(dnr^2)$ , and for the Tucker tensor decomposition, it scales with  $\mathcal{O}(r^d + ndr^{d-1})$ . The cross approximation algorithms **TT-CUR-DEIM** for tensor train and **DEIM-FS** for Tucker tensor decompositions are employed, respectively. Similar to our findings in [1], both **TT-CUR-DEIM** and **DEIM-FS** are designed to be agnostic to the type of nonlinearity encountered (e.g., fractional, exponential, etc.). (ii) Implementing these methods is straightforward, as they require only the evaluation of the time-discrete FOM at strategically selected entries. (iii) This approach to time integration is robust in the presence of small singular values and it is extended for high-order explicit time integration schemes, such as the fourth-order Runge-Kutta (RK4). The algorithm is also rank-adaptive, effectively adjusting the rank of the approximation on the fly.

The remainder of the paper is organized as follows. The methodologies are discussed in Section 2, demonstrations and results are presented in Section 3, and the conclusions follow in Section 4. Supplementary methodologies are discussed in the Appendix section.

## 2. Methodology

### 2.1. Definitions and notations

We introduce the notations used for vectors, matrices, and tensors in this paper. Vectors are denoted in bold lowercase letters (e.g.  $\mathbf{a}$ ), matrices are denoted by bold uppercase letters (e.g.  $\mathbf{A}$ ), and tensors by uppercase letters (e.g.  $A$ ). The symbol  $\times_n$  is used to denote the  $n$ -mode product. The  $n$ -mode product of a tensor  $A \in \mathbb{R}^{n_1 \times n_2 \times \dots \times n_d}$  with a matrix  $\mathbf{M} \in \mathbb{R}^{J \times n_n}$  is obtained by  $A \times_n \mathbf{M}$  and is of size  $n_1 \times \dots \times n_{n-1} \times J \times n_{n+1} \times \dots \times n_d$ . We denote the unfolding of tensor  $A$  along its  $n$ -th mode with  $A_{(n)}$ . Unfolding a tensor involves reshaping its elements in such a way that results in a matrix instead of a tensor. For example, a tensor of size  $4 \times 6 \times 7$  can be unfolded along the second

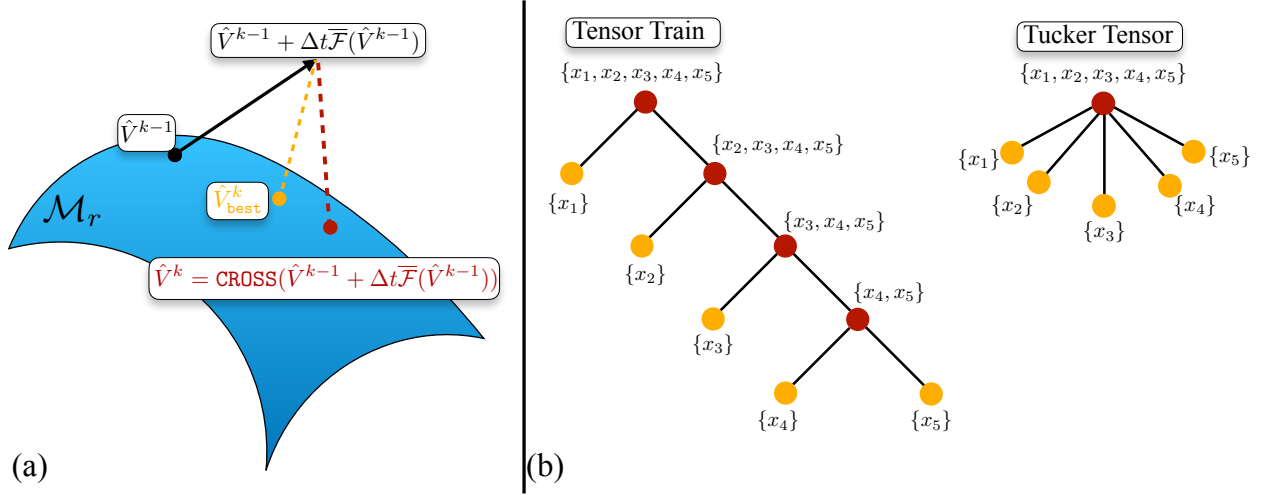


Figure 1: (a) Schematic of the cross algorithm for time integration of tensor differential equations on the manifold of low-rank tensors without utilizing tangent space projection. (b) Tensor Train and Tucker tensor trees for  $v(x_1, x_2, x_3, x_4, x_5)$ .

axis as a matrix of size  $6 \times 28$  [2]. The Frobenius norm of a tensor is shown by  $\|A\|_F$  and is defined as:

$$\|A\|_F = \sqrt{\sum_{i_1=1}^{n_1} \sum_{i_2=1}^{n_2} \cdots \sum_{i_d=1}^{n_d} a_{i_1 i_2 \dots i_d}^2}, \quad (1)$$

where  $a_{n_1 n_2 \dots n_d}$  are the entries of tensor  $A$ . MATLAB indexing notation is used where  $\mathbf{A}(\mathbf{p}, :)$  selects all columns at the  $\mathbf{p}$  rows and  $\mathbf{A}(:, \mathbf{p})$  selects all rows at the  $\mathbf{p}$  columns of matrix  $\mathbf{A}$  and  $\mathbf{p} = [p_1, p_2, \dots, p_q]$  is the integer vector containing the selected indices. We use typewriter font to denote algorithms and MATLAB functions, e.g., `SVD` and `DEIM` and `reshape`. We also use MATLAB notation for computing the SVD of a matrix. For example, consider for  $\mathbf{A} \in \mathbb{R}^{m \times n}$ . Then  $[\mathbf{U}, \mathbf{\Sigma}, \mathbf{V}] = \text{SVD}(\mathbf{A}, r)$  means computing the SVD of  $\mathbf{A}$  and truncating at rank  $r$ , where  $r < m$  and  $r < n$ ,  $\mathbf{U} \in \mathbb{R}^{n \times r}$  is the matrix of left singular vectors,  $\mathbf{\Sigma} \in \mathbb{R}^{r \times r}$  is the matrix of singular values and  $\mathbf{V} \in \mathbb{R}^{m \times r}$  is the matrix of right singular vectors. If any of the singular matrices are not needed, the symbol  $(\sim)$  is used. For example,  $[\mathbf{U}, \sim, \sim] = \text{SVD}(\mathbf{A}, r)$  returns only the first  $r$  left singular vectors. We denote sets using square brackets  $[ ]$ , where set  $[a_i]$ ,  $i = 1, \dots, m$  includes  $[a_1, a_2, \dots, a_m]$ .

**Definition 1 (Tucker tensor format).** A tensor  $\hat{V} \in \mathbb{R}^{n_1 \times \dots \times n_d}$  is expressed in Tucker tensor form as

$$\hat{V}(i_1, \dots, i_d) = \sum_{\alpha_1=1}^{r_1} \cdots \sum_{\alpha_d=1}^{r_d} G(\alpha_1, \dots, \alpha_d) \cdot \mathbf{U}_1(i_1, \alpha_1) \cdots \mathbf{U}_d(i_d, \alpha_d), \quad (2)$$

where  $G \in \mathbb{R}^{r_1 \times \dots \times r_d}$  is the core tensor,  $\mathbf{U}_i \in \mathbb{R}^{n_i \times r_i}$  are the factor matrices, and  $\mathbf{r} = (r_1, \dots, r_d)$  are Tucker tensor multi-rank, which we denote with  $TU\text{-rank}(\hat{V}) = \mathbf{r}$ .

**Definition 2 (Tensor train format).** A tensor  $\hat{V} \in \mathbb{R}^{n_1 \times \dots \times n_d}$  is expressed in tensor train form as

$$\hat{V}(i_1, \dots, i_d) = \sum_{\alpha_1=1}^{r_1} \cdots \sum_{\alpha_{d-1}=1}^{r_{d-1}} G_1(1, i_1, \alpha_1) \cdot G_2(\alpha_1, i_2, \alpha_2) \cdots G_d(\alpha_{d-1}, i_d, 1) \quad (3)$$

where  $G_i \in \mathbb{R}^{r_{i-1} \times n_i \times r_i}$  are the core tensors, and  $r_0 = r_d = 1$ . Moreover,  $\mathbf{r} = (r_1, \dots, r_{d-1})$  are tensor train compression ranks, which we denote with  $TT\text{-rank}(\hat{V}) = \mathbf{r}$ .

**Definition 3 (Low-rank tensor manifolds).** The low-rank tensor manifold  $\mathcal{M}_r$  is defined as the set

$$\mathcal{M}_r = \{\hat{V} \in \mathbb{R}^{n_1 \times \dots \times n_d} : \text{rank}(\hat{V}) = \mathbf{r}\},$$

of tensors of fixed rank  $r$ . Any member of the set  $\mathcal{M}_r$  is denoted by a hat symbol ( $\hat{\cdot}$ ), e.g.,  $\hat{V}$ . We use  $\mathcal{M}_r$  to generically refer to low-rank manifolds, represented by either Tucker tensors or tensor trains, with the specific manifold being understood from the context.

To simplify computational complexity analyses, we assume  $n \sim \mathcal{O}(n_i)$  and  $r \sim \mathcal{O}(r_i)$ . Therefore, the full-dimensional tensor  $V \in \mathbb{R}^{n_1 \times \dots \times n_d}$  has  $\mathcal{O}(n^d)$  entries, the rank- $r$  Tucker tensor approximation of  $V$  reduces the number of entries to  $\mathcal{O}(r^d + rdn)$  and the rank- $r$  tensor train approximation of  $V$  reduces the number of entries to  $\mathcal{O}(r^2 dn)$ .

**Definition 4 (Interpolatory CUR decomposition).** The interpolatory CUR decomposition of matrix  $\mathbf{V} \in \mathbb{R}^{n_1 \times n_2}$  is a rank- $r$  approximation of  $\mathbf{V}$  in the form of  $\hat{\mathbf{V}} = \mathbf{C}\mathbf{U}\mathbf{R}$ , where  $\mathbf{C} = \mathbf{V}(:, \mathbf{j}) \in \mathbb{R}^{n_1 \times r}$  are some  $r$  columns of  $\mathbf{V}$  and  $\mathbf{R} = \mathbf{V}(\mathbf{i}, :) \in \mathbb{R}^{r \times n_2}$  are some  $r$  rows of  $\mathbf{V}$ . The matrix  $\mathbf{U} = (\mathbf{V}(\mathbf{i}, \mathbf{j}))^{-1} \in \mathbb{R}^{r \times r}$ .

## 2.2. Time integration using tangent spaces

We consider a general PDE given by:

$$\frac{\partial v(\mathbf{x}, t)}{\partial t} = f(v(\mathbf{x}, t)), \quad (4)$$

augmented with appropriate initial and boundary conditions. Here  $\mathbf{x} = (x_1, x_2, \dots, x_d) \in \mathbb{R}^d$ ,  $t$  is time,  $f$  is a general nonlinear differential operator, and  $d$  is the dimension of the problem. Discretizing the differential operators of Eq. (4) in  $\mathbf{x}$  using a method of lines results in the following TDE:

$$\frac{dV}{dt} = \mathcal{F}(V), \quad (5)$$

where  $V(t) \in \mathbb{R}^{n_1 \times n_2 \times \dots \times n_d}$  is the solution tensor and  $\mathcal{F}(\sim)$  is the discrete representation of  $f(\sim)$ . Here,  $n_1, n_2, \dots, n_d$  are the number of the discretized degrees of freedom along each mode of the tensor. We refer to Eq. (5) as the full-order model (FOM).

The degrees of freedom of the FOM increase exponentially as  $d$  grows. Tensor low-rank approximations can mitigate this issue via low-rank approximation of  $V(t)$  by constraining the solution of the above TDE to a manifold of low-rank tensors. In this work, we consider two tensor low-rank approximation schemes: Tucker tensor and tensor train decompositions. We seek an approximation  $\hat{V}(t)$  to the exact solution  $V(t)$  where  $\hat{V}(t)$  is the constrained solution to low-rank Tucker tensor or tensor train manifold.

Substituting the low-rank approximation  $\hat{V}(t)$  into Eq. (5) results in a residual equal to:

$$\mathcal{R}(\dot{\hat{V}}) = \|\dot{\hat{V}} - \mathcal{F}(\hat{V})\|_F. \quad (6)$$

The low-rank tensor train and Tucker tensor approximation of Eq. (5) is obtained by minimization of the above residual with the constraint that  $\hat{V} \in \mathcal{T}_{\hat{V}}\mathcal{M}_r$ , which results in:

$$\dot{\hat{V}} = \mathcal{P}_{\mathcal{T}_{\hat{V}}}\mathcal{F}(\hat{V}), \quad (7)$$

where  $\mathcal{T}_{\hat{V}}\mathcal{M}_r$  is the tangent space of the manifold  $\mathcal{M}_r$  at  $\hat{V} \in \mathcal{M}_r$ , and  $\mathcal{P}_{\mathcal{T}_{\hat{V}}}$  is the orthogonal projection onto the tangent space  $\mathcal{T}_{\hat{V}}$  at  $\hat{V}$ . The DLRA evolution equations for the Tucker tensor form are presented in [17] and for the tensor train in [41].

Although, the scheme of Eq. (7) has the potential to significantly reduce the computational cost of solving high-dimensional TDEs, there are still several challenges for most practical problems of interest. As outlined in the Introduction, computing  $F = \mathcal{F}(V) \in \mathbb{R}^{n_1 \times \dots \times n_d}$  in many nonlinear problems requires  $\mathcal{O}(n^d)$  operations, mirroring the computational complexity of solving the FOM. Even in linear TDEs, a substantial number of terms on the right-hand side may result in a large exact rank for  $F$ . While it is possible to achieve the reduction offered by Tucker tensor and tensor train decompositions in special cases of linear and quadratic nonlinear TDEs, this involves a highly intrusive and meticulous treatment of the right-hand side terms to avoid storing the full-rank or high-rank tensors. Moreover, the projection of Eq. (7) may encounter computational stability issues since the derived DLRA evolution equations from Eq. (7) include the inverse of auto-correlation matrices. When the tensor solution incorporates small singular values, the auto-correlation matrices become ill-conditioned. This phenomenon is attributed to the curvature of the tensor manifold  $\mathcal{M}_r$ , which is inversely proportional to the smallest singular value [29, 42].

### 2.3. Time discrete variational principle and cross low-rank approximation

To address the challenges of the DLRA, we propose a methodology that is inspired by our previous work on matrix low-rank approximation [1]. In particular, we consider the temporal discretization of the FOM:

$$V^k = \hat{V}^{k-1} + \Delta t \overline{\mathcal{F}}(\hat{V}^{k-1}), \quad (8)$$

where  $\Delta t$  is the time-step size, and  $\overline{\mathcal{F}}$  depends on the temporal discretization that could be a multi-step or a Runge-Kutta-based scheme. For example, the first-order explicit Euler method is simply  $\overline{\mathcal{F}}(\hat{V}^{k-1}) = \mathcal{F}(\hat{V}^{k-1})$ . It should be noted that since  $\hat{V}^{k-1} + \Delta t \overline{\mathcal{F}}(\hat{V}^{k-1})$  is calculated based on Eq. (8) the solution at the previous time instant is in the low-rank form. Depending on the type of  $\mathcal{F}(\sim)$ , the tensor  $V^k$  is generally of higher rank or full rank. For example, if  $\mathcal{F}(\sim)$  has non-polynomial nonlinearity,  $\mathcal{F}(\hat{V}^{k-1})$  is full rank even when  $\hat{V}^{k-1}$  is low rank. In fact, except for a few rare cases, one forward step of Eq. (8) moves  $V^k$  out of the rank- $r$  manifold. Thus, to keep the solution of the TDE on the manifold of rank- $r$ , a rank truncation is required to project the solution back onto  $\mathcal{M}_r$  at every single time step. Ideally, we need to approximate  $V^k$  with a rank- $r$  tensor  $\hat{V}^k$ , such that:

$$V^k = \hat{V}^k + E^k, \quad (9)$$

where  $E^k$  is the error of the low-rank approximation. The best approximation can be found by minimizing the norm of the residual [31, 35]:

$$\min \mathcal{J}(\hat{V}^k) = \|V^k - \hat{V}^k\|_F^2, \quad \text{such that } \hat{V}^k \in \mathcal{M}_r. \quad (10)$$

We refer to the minimization described above as the time-discrete variational principle. The advantages of the time-discrete formulation is that: (i) it is robust in the presence of small or zero singular values; (ii) it can retain the temporal accuracy of the FOM. Solving this minimization problem is quite costly, not only because it necessitates an iterative algorithm but more critically because it involves forming the full or high-rank tensor  $V^k$ . Avoiding this expense—both in terms of memory requirements and computational costs (flops)—is the very reason we pursue low-rank approximation in the first place.

Another approach to finding a near-optimal  $\hat{V}^k$  involves using tensor train SVD (TT-SVD) for tensor train decomposition, or higher-order SVD (HOSVD) for Tucker tensor decomposition. Although neither of these approaches is iterative, any SVD-based methods, including randomized algorithms, require computing the entries of  $V^k$  when  $V^k$  is of full rank, for instance, for non-polynomial nonlinear  $\mathcal{F}(\sim)$ .

Nearly identical issues are also encountered for solving nonlinear MDEs on low-rank manifolds. We recently proposed a CUR algorithm for the low-rank approximation of MDEs [1]. Specifically, the proposed algorithm in [1] approximates the solution of MDE using:

$$\hat{\mathbf{V}}^k = \text{CUR}(\hat{\mathbf{V}}^{k-1} + \Delta t \bar{\mathcal{F}}(\hat{\mathbf{V}}^{k-1})), \quad (11)$$

where we proposed an interpolatory CUR algorithm based on DEIM. In this work, we demonstrate that the identical approach can be applied to both Tucker tensor and tensor train approximations. Specifically, the solution at the next time step can be constructed using a cross approximation as shown below:

$$\hat{V}^k = \text{CROSS}(\hat{V}^{k-1} + \Delta t \bar{\mathcal{F}}(\hat{V}^{k-1})), \quad (12)$$

where we use cross algorithms to directly construct a low-rank approximation at the next time step. The accuracy and efficiency of the cross algorithms depend critically on how the fibers are selected. There are excellent choices for cross algorithms for both tensor train and Tucker tensor decomposition that are appropriate for time integration; see for example [8, 39, 43]. Recently we presented a Tucker cross algorithm [39], where the fibers are selected based on the DEIM algorithm. This algorithm from [39] is presented in Appendix B for convenience. We refer to this algorithm as DEIM-FS, where FS stands for fiber sampling. For the tensor train, we present TT-CUR-DEIM - a new tensor train cross algorithm based on DEIM. This algorithm is presented in detail in Appendix C. Therefore, the time integration schemes of the TDE on Tucker and tensor train low-rank manifold can be simply expressed as:

$$\text{Tucker tensor: } \hat{V}^k = \text{DEIM-FS}(\hat{V}^{k-1} + \Delta t \bar{\mathcal{F}}(\hat{V}^{k-1})), \quad (13a)$$

$$\text{Tensor train: } \hat{V}^k = \text{TT-CUR-DEIM}(\hat{V}^{k-1} + \Delta t \bar{\mathcal{F}}(\hat{V}^{k-1})). \quad (13b)$$

The above algorithm is remarkably simple and can be explained in the following steps: The tensor  $V^k = \hat{V}^{k-1} + \Delta t \bar{\mathcal{F}}(\hat{V}^{k-1})$  represents the solution of the FOM at time step  $k$ , with the solution at the previous time step,  $k-1$ , set as the low-rank tensor. However,  $V^k$ , which would be high or full-rank, is never actually formed. Instead, the low-rank tensor at time step  $k$  is obtained by performing a rank truncation using a cross algorithm, which judiciously evaluates  $V^k$  at sparse entries.

In the following, we list the advantages of the above time-integration algorithm:

- **Computational Cost:** For tensor train decomposition, TT-CUR-DEIM only samples  $r^2dn$  entries of the cross algorithm regardless of the type of nonlinearity of  $\mathcal{F}(\sim)$ . This means that the TT-CUR-DEIM evaluates the right-hand side function at the minimum number of entries possible for a rank- $r$  approximation, which is significantly smaller than the full-size tensor, which requires  $n^d$  function evaluations. The algorithm is also memory efficient and has the storage complexity of  $\mathcal{O}(r^2dn)$ . The DEIM-FS algorithm has memory and cost complexity of  $\mathcal{O}(r^d + ndr^{d-1})$ .
- **Ill-Conditioning:** The inversion of the singular value matrix is not needed in the above algorithm and it is robust in the presence of small or zero singular values. Similar to what was shown in [1], the tensor DEIM-based cross algorithms are well-conditioned. The same is true for maxvol cross algorithms [8, 44].
- **High-Order Temporal Integration:** The algorithm inherits the temporal accuracy of the scheme used for temporal integration. Details of the Runge-Kutta time integration scheme are presented in Section 2.4.2. As shown in Figures 3a and 3b, the time integration method presented for both tensor train and Tucker tensor decompositions retains the fourth-order temporal accuracy of RK4 for nonlinear TDEs.
- **Intrusiveness:** The above algorithm is remarkably easy to implement, mainly because it only evaluates the full-order model at judiciously chosen entries. It does not involve tangent space projections, nor does it require term-by-term treatment of the low-rank tensor, both of which can be quite involved depending on the TDE. The cross algorithms are implemented only once and are straightforward to implement. For the most part, they are agnostic to the type of TDEs being applied. All the examples in this paper utilize the same cross algorithm.
- **Rank Adaptivity:** It is straightforward to perform rank adaptivity using the cross algorithms, which involves sampling additional or fewer fibers if rank addition or removal criterion is triggered. We present the details of rank adaptivity in Section 2.4.1.

#### 2.4. Tucker tensor and tensor train cross algorithms

We use the DEIM-FS algorithm from [39] as a Tucker tensor cross algorithm. The algorithm is presented in Appendix B for convenience. We refer the reader to [39] for more details on DEIM-FS algorithm.

In Appendix C, we present TT-CUR-DEIM (*iterative*), a cross algorithm for tensor train based on DEIM. The DEIM algorithm requires the singular vectors to determine the interpolation points. However, these singular vectors are not available in most applications. In Appendix C, we present an iterative TT-CUR-DEIM cross algorithm, which does not require access to singular vectors. As a result, the TT-CUR-DEIM (*iterative*) can be seen as a black box cross algorithm for tensor train similar to cross algorithms based on maxvol [8].

However, for the time integration of TDE on low-rank manifolds, we can leverage the information from the previous timestep to eliminate the iterative process of the TT-CUR-DEIM. This approach is similar to our method for solving matrix differential equations, as explained in [1]. Specifically, in the time integration of  $V^k$ , the left-to-right nested indices determined in the previous timestep can be reused in the current timestep. We apply an analogous procedure for time integration in the low-rank Tucker form, where the fiber indices from the previous timestep are used. This enables obtaining a low-rank tensor train and Tucker tensor approximation of  $V^k$

without any iteration. In practice, utilizing the indices from the previous timestep yields excellent performance. The accuracy difference when TT-CUR-DEIM is used iteratively is negligible. A similar approach was employed in [1, 25, 39], where information from the previous timestep is utilized in the current timestep to solve matrix and tensor differential equations. At  $t = 0$ , TT-CUR-DEIM may be used iteratively to determine the left or right-nested indices.

The details of TT-CUR-DEIM for time integration of TDEs are summarized in Algorithm 3. This algorithm is presented for a three-dimensional tensor for simplicity, but it can easily be generalized to higher-dimensional tensors.

#### 2.4.1. Rank adaptivity

The proposed time integration algorithm can be augmented with rank adaptivity, enabling on-the-fly control of the error in the low-rank approximation. By utilizing this feature, we can maintain the desired level of accuracy while avoiding unnecessary computations by overapproximation. To this end, we define an error proxy as:

$$\epsilon_z = \frac{\min(\Sigma_z)}{\|\Sigma_z\|_F} \quad z = 1, \dots, d-1, \quad (14)$$

where  $\Sigma_z$  is the matrix of singular values of  $V_z$ , i.e.  $[\sim, \Sigma_z, \sim] = \text{SVD}(V_z, r_z)$ ,  $z = 1, \dots, d-1$ . Here,  $V_z$  is a subtensor. See Appendix C for more details on the notation. This quantity measures the relative contribution of the  $r$ -th rank. The rank  $r_z$  is adjusted or remains unchanged to maintain  $\epsilon$  within a desired range,  $\epsilon_l \leq \epsilon_z \leq \epsilon_u$ , where  $\epsilon_l$  and  $\epsilon_u$  are user-specified lower and upper thresholds. In case  $\epsilon_z < \epsilon_l$ , the rank is reduced by one such that the new rank is  $r'_z = r_z - 1$ . Once the new rank is determined, the DEIM-selected indices  $(\mathbf{i}_1, \mathbf{i}_2, \dots, \mathbf{i}_{d-1})$  are truncated to retain the first  $r'_z$  components. On the other hand, when  $\epsilon_z > \epsilon_u$ , the new rank is obtained as  $r'_z = r_z + 1$ . The rank is increased by sampling more indices and updating  $\mathbf{i}_1, \mathbf{i}_2, \dots, \mathbf{i}_{d-1}$ . Since DEIM only provides sampling points equal to the number of the columns of the left singular matrix (i.e.  $\mathbf{U}_1$  and  $\mathbf{U}_2$ ), we perform oversampling using GappyPOD+E algorithm presented in [45]. Although any sparse selection method can be used, it has been demonstrated that GappyPOD+E outperforms alternative approaches such as random sampling or leverage scores in performance [46]. By utilizing the GappyPOD+E, we add  $m$  more indices to the index sets  $\mathbf{i}_1, \mathbf{i}_2, \dots, \mathbf{i}_{d-1}$ , where  $m \geq 1$  is an arbitrary number. As  $m$  increases, the low-rank approximation error will decrease, however, in practice,  $m = 5$  can capture the desired level of accuracy.

#### 2.4.2. High-order Runge-Kutta temporal integration

Up until this point, we have regarded  $V^k = \hat{V}^{k-1} + \Delta t \bar{F}$  as a tensor of size  $n_1 \times n_2 \times \dots \times n_d$  derived from an explicit Runge-Kutta temporal discretization of Eq. (5). As mentioned in Appendix D, depending on the employed numerical scheme for spatial discretization, the set of adjacent points (e.g.,  $j_{a2}^{(\alpha_1)}$ ) may be required for computing  $V_1^k, V_2^k, \dots, V_d^k$ . Hence, for higher-order time integration schemes, such as fourth-order Runge-Kutta, these dependencies on adjacent points can grow exponentially with the number of Runge-Kutta stages. This issue was similarly encountered in solving matrix differential equations [1]. In [1], a CUR approximation of  $\mathbf{K}^{(i+1)} = F(\hat{\mathbf{V}} + \beta \Delta t \mathbf{K}^{(i)})$  is constructed at each stage, where  $\mathbf{K}^{(i)}$  is the output of the RK at stage  $i$ . We extend the same solution to tensors as explained below. For simplicity, we consider the second-order explicit Runge-Kutta scheme for a three-dimensional tensor, i.e.,  $d = 3$ . In this case:

$$\begin{aligned}
K^{(1)} &= \mathcal{F}(\hat{V}^{k-1}), \\
K^{(2)} &= \mathcal{F}\left(\hat{V}^{k-1} + \frac{1}{2}\Delta t K^{(1)}\right).
\end{aligned}$$

To compute  $\hat{V}_1^k$ , first, we can compute the first stage of time integration  $K_1^{(1)} = \mathcal{F}(\hat{V}_1^{k-1})$  at the DEIM-selected entries, where  $K_1^{(1)} \in \mathbb{R}^{1 \times n_1 \times r_1}$  is the subtensor of  $K^{(1)}$  at the DEIM-selected entries:

$$K_1^{(1)}(1, :, \alpha_1) = \mathcal{F}\left(G_1^{k-1} G_2^{k-1}(:, [j_2^{(\alpha_1)}, j_{a_2}^{(\alpha_1)}], :) G_3^{k-1}(:, [j_3^{(\alpha_1)}, j_{a_3}^{(\alpha_1)}], :)\right), \quad \alpha_1 = 1, \dots, r_1. \quad (15)$$

In case the explicit Euler method is used,  $\bar{F}_1 = K_1^{(1)}$ , and no further steps are required. If a higher-order temporal integration such as RK2 is employed, the second stage needs to be calculated at all cross-selected entries:

$$K_1^{(2)} = \mathcal{F}\left(\hat{V}_1^{k-1} + \frac{1}{2}\Delta t K_1^{(1)}\right). \quad (16)$$

To calculate  $K_1^{(2)}$ , we need to evaluate  $\hat{V}_1^{k-1}$  and  $K_1^{(1)}$  at the index sets  $[j_2^{(\alpha_1)}]$  and  $[j_3^{(\alpha_1)}]$ , as well as their adjacent points ( $[j_{a_2}^{(\alpha_1)}]$ ,  $[j_{a_3}^{(\alpha_1)}]$ ). The evaluation of  $K_1^{(1)}$  at the adjacent points leads to an increase in adjacent entries since the adjacent points (i.e.,  $[j_{a_2}^{(\alpha_1)}]$ ,  $[j_{a_3}^{(\alpha_1)}]$ ) have their own adjacent points. These adjacent of adjacent points are required to compute  $K_1^{(1)}$ . This process rapidly becomes overwhelming, particularly with the addition of more stages to the integration scheme. Accordingly, for higher-order schemes (e.g., RK4), the efficacy provided by the presented algorithm diminishes, leading to an increasingly intricate implementation. To address these challenges, we construct a low-rank approximation to  $K^{(1)}$  and  $K^{(2)}$ . This can be done via the same cross algorithm: Therefore, we can approximate  $K^{(i)}$  with:

$$\hat{K}^{(i+1)} = \text{TT-CUR-DEIM}(\mathcal{F}(\hat{V}^{k-1} + \beta \Delta t \hat{K}^{(i)})), \quad (17a)$$

$$\hat{K}^{(i+1)} = \text{DEIM-FS}(\mathcal{F}(\hat{V}^{k-1} + \beta \Delta t \hat{K}^{(i)})). \quad (17b)$$

This step does not require any additional function sampling and therefore does not change the computational complexity of the algorithm. Once the low-rank approximation for each stage of time integration is obtained, we can evaluate  $\hat{K}^{(i)}$  at any arbitrary index sets (e.g.  $[j_{a_2}^{(\alpha_1)}]$ , and  $[j_{a_3}^{(\alpha_1)}]$ ) in a cost-efficient way. Note that these constructed low-rank approximations for  $K^{(1)}$  and  $K^{(2)}$  are not just used for computing  $V_1^k$ . We also use these low-rank approximations for calculating  $V_2^k$  and  $V_3^k$  by evaluating at their corresponding index sets. Although the second-order Runge–Kutta scheme is used for demonstration, this approach is easily extended to higher-order Runge–Kutta methods. Similar approaches were adopted to construct a low-rank approximation of  $K^{(i)}$  in solving nonlinear matrix and tensor differential equations [1, 25, 39].

### 3. Demonstrations

#### 3.1. Toy Examples

As the first example, we consider two three-dimensional functions as shown below:

$$\mathcal{F}_1(x_1, x_2, x_3) = e^{-4(x_1 x_2 x_3)^2} \quad x_1, x_2, x_3 \in [-1, 1], \quad (18a)$$

$$\mathcal{F}_2(x_1, x_2, x_3) = \frac{1}{(x_1^b + x_2^b + x_3^b)^{1/b}} \quad x_1, x_3 \in [1, 200] \quad x_2 \in [1, 300]. \quad (18b)$$

---

**Algorithm 1:** Rank adaptive low-rank tensor train time integration cross algorithm

---

**Input:**  $\tilde{G}_0, \tilde{G}_1, \tilde{G}_2$ : Core tensors of the tensor train decomposition from the previous time step.

$[j_2^{(\alpha_1)}], [j_3^{(\alpha_1)}], [j_3^{(\alpha_2)}]$ : The indices of the selected fibers from the previous time step.

**Output:**  $G_0, G_1, G_2$ : Core tensors of the tensor train decomposition in the current time step

```

1  $\hat{V}_1(1, :, \alpha_1) = \tilde{G}_1 \tilde{G}_2(:, j_2^{(\alpha_1)}, :) \tilde{G}_3(:, j_3^{(\alpha_1)}, :), \quad \alpha_1 = 1, \dots, r_1$ 
2  $\bar{F}_1(1, :, \alpha_1) = \mathcal{F}(\tilde{G}_1 \tilde{G}_2(:, [j_2^{(\alpha_1)}, j_{a_2}^{(\alpha_1)}], :) \tilde{G}_3(:, [j_3^{(\alpha_1)}, j_{a_3}^{(\alpha_1)}], :)), \quad \alpha_1 = 1, \dots, r_1$ 
3  $V_1 = \hat{V}_1 + \Delta t \bar{F}_1$ 
4  $[\mathbf{U}_1, \mathbf{\Sigma}_1, \sim] = \text{SVD}(V_1, r_1)$ 
5  $\mathbf{i}_1 = \text{DEIM}(\mathbf{U}_1), \quad \mathbf{i}_1 = [i_1^{(\alpha_1)}], \quad \alpha_1 = 1, \dots, r_1$ 
6  $G_1 = \mathbf{U}_1 (\mathbf{U}_1(\mathbf{i}_1, :))^{-1}$ 
7  $\hat{V}_2(\alpha_1, :, \alpha_2) = \tilde{G}_1(:, i_1^{(\alpha_1)}, :) \tilde{G}_2(:, j_3^{(\alpha_2)}, :), \quad \alpha_1 = 1, \dots, r_1, \quad \alpha_2 = 1, \dots, r_2$ 
8  $\bar{F}_2(\alpha_1, :, \alpha_2) = \mathcal{F}(\tilde{G}_1(:, [i_1^{(\alpha_1)}, i_{a_1}^{(\alpha_1)}], :) \tilde{G}_2(:, [j_3^{(\alpha_2)}, j_{a_3}^{(\alpha_2)}], :)), \quad \alpha_1 = 1, \dots, r_1, \quad \alpha_2 = 1, \dots, r_2$ 
9  $V_2 = \hat{V}_2 + \Delta t \bar{F}_2$ 
10  $[\mathbf{U}_2, \mathbf{\Sigma}_2, \sim] = \text{SVD}(\text{reshape}(V_2, [r_1 n_2, q_2])), r_2)$ 
11  $\mathbf{i}_2 = \text{DEIM}(\mathbf{U}_2), \quad \mathbf{i}_2 = \{[i_1^{(\alpha_2)}], [i_2^{(\alpha_2)}]\}, \quad \alpha_2 = 1, \dots, r_2$ 
12  $G_2 = \text{reshape}(\mathbf{U}_2 (\mathbf{U}_2(\mathbf{i}_2, :))^{-1}, [r_1, n_2, r_2])$ 
13  $\hat{V}_3(\alpha_2, :, 1) = \tilde{G}_1(:, i_1^{(\alpha_2)}, :) \tilde{G}_2(:, i_2^{(\alpha_2)}, :) \tilde{G}_3, \quad \alpha_2 = 1, \dots, r_2$ 
14  $\bar{F}_3(\alpha_2, :, 1) = \mathcal{F}(\tilde{G}_1(:, [i_1^{(\alpha_2)}, i_{a_1}^{(\alpha_2)}], :) \tilde{G}_2(:, [i_2^{(\alpha_2)}, i_{a_2}^{(\alpha_2)}], :) \tilde{G}_3), \quad \alpha_2 = 1, \dots, r_2$ 
15  $G_3 = V_3 = \hat{V}_3 + \Delta t \bar{F}_3$ 
16  $\epsilon_z = \frac{\min(\mathbf{\Sigma}_z)}{\|\mathbf{\Sigma}_z\|_F}, \quad z = 1, 2$ 
17 if  $\epsilon_z > \epsilon_u$  then
    |  $r'_z = r_z + 1, \quad z = 1, 2$ 
    | Do oversampling and update  $\mathbf{i}_1 \in \mathbb{I}^{r_1+m}, \mathbf{i}_2 \in \mathbb{I}^{r_2+m}$ 
else if  $\epsilon_z < \epsilon_l$  then
    |  $r'_z = r_z - 1, \quad z = 1, 2$ 
    | Truncate  $\mathbf{i}_1, \mathbf{i}_2$  at the updated ranks
else
    |  $r'_z = r_z, \quad z = 1, 2$ 
18  $[j_2^{(\alpha_1)}] = [i_2^{(\alpha_2)}]; \quad [j_3^{(\alpha_1)}] = [i_1^{(\alpha_2)}]; \quad [j_3^{(\alpha_2)}] = [i_1^{(\alpha_1)}]$ 
19  $r_1 = r'_2; \quad r_2 = r'_1$ 
20  $\tilde{G}_0 = \text{permute}(G_3, [3, 2, 1]), \quad \tilde{G}_1 = \text{permute}(G_1, [3, 2, 1]), \quad \tilde{G}_3 = \text{permute}(G_0, [3, 2, 1])$ 

```

---

By evaluating  $\mathcal{F}_1(x_1, x_2, x_3)$  at 100 equally spaced points for each of  $x_1, x_2$ , and  $x_3$  within their respective domains, we obtain  $F_1$ , a tensor of size  $100 \times 100 \times 100$ . Similarly, evaluating  $\mathcal{F}_2(x_1, x_2, x_3)$  on an equally spaced grid in each direction results in a tensor  $F_2 \in \mathbb{R}^{200 \times 300 \times 200}$ . Two choices of  $b = 3$  and  $b = 5$  are considered for  $F_2$ . To compare the performance of the DEIM and maxvol algorithms in efficient fiber selection,  $F_1$  and  $F_2$  are approximated using TT-CUR-DEIM and TT-Cross-maxvol, respectively. Then, the error between the approximated tensors and the actual tensors is calculated. The low-rank approximation error is defined as:

$$\mathcal{E} = \|\hat{F} - F\|_F,$$

where  $\hat{F}$  denotes the low-rank tensor train approximation of  $F$ . For both methods, we consider  $r_1 = r_2 = r_3 = r$ . Figures 2a and 2b show the low-rank approximation error versus rank ( $r$ ) for  $F_1$  and  $F_2$ , respectively. As shown in these figures, the error of TT-Cross-maxvol algorithm closely follows the TT-CUR-DEIM error. The results demonstrate that both DEIM and maxvol methods are performing comparably.

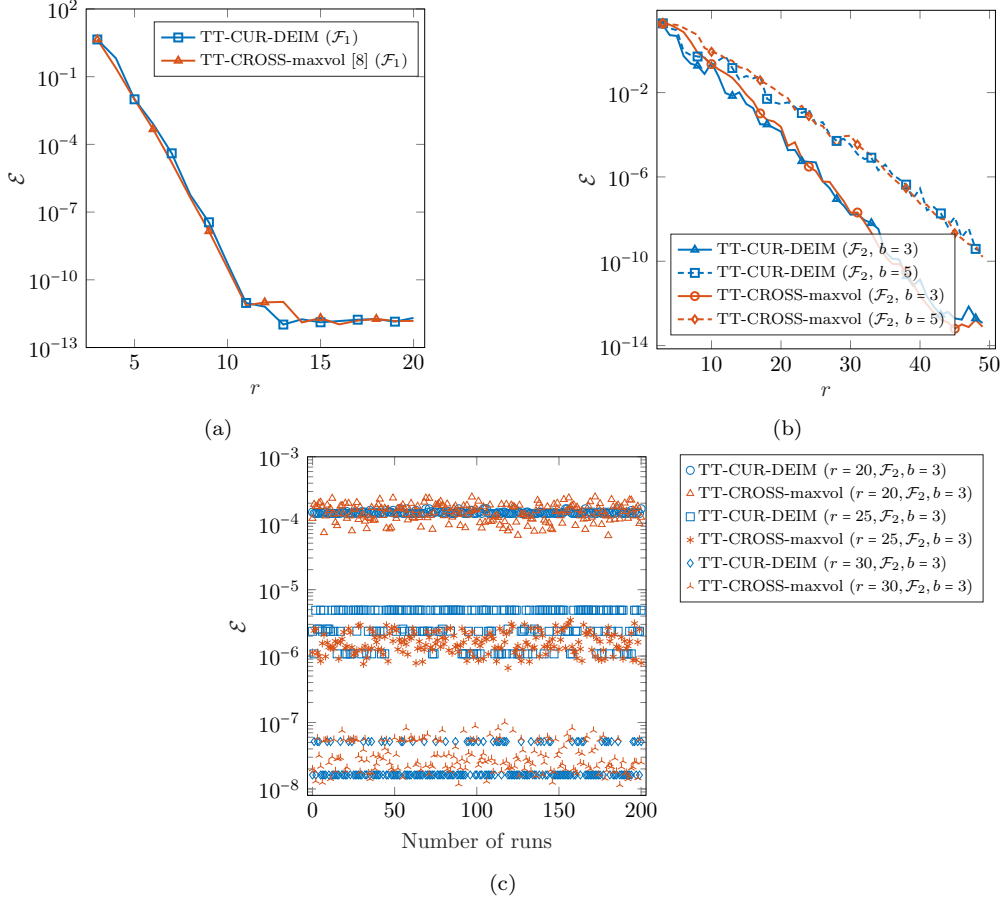


Figure 2: Toy Examples: Comparison of the TT-CUR-DEIM and TT-Cross-maxvol: (a) Approximation error of  $F_1$  versus rank; (b) Approximation error of  $F_2$ , ( $b = 3, 5$ ) versus rank; (c) Effect of random fiber initialization on the approximation error of  $F_2$ , ( $b = 3$ ) for three different ranks ( $r = 20$ ,  $r = 25$ ,  $r = 30$ )

In both TT-CUR-DEIM and TT-Cross-maxvol methods, the initial right-nested indices are selected randomly. We conducted a study to examine the effect of different initialization on the accuracy of the low-rank approximations. Figure 2c depicts the approximation error of  $F_2$  ( $b = 3$ ) obtained from 200 random initializations of both TT-CUR-DEIM and TT-Cross-maxvol algorithms. Overall both techniques show similar errors but DEIM shows a smaller variance in most cases considered. Figure 2c illustrates that depending on the rank and initialization, one of the algorithms may result in a slightly lower error compared to the other. However, in general, they both exhibit similar accuracy. In summary, our observation reveals that DEIM and maxvol are competitive algorithms for fiber selection and the computational complexity of both methods scales with  $\mathcal{O}(nr)$ .

### 3.2. Three-dimensional nonlinear TDE

One of the important advantages of applying residual minimization at the time discrete level is that the resulting low-rank approximation inherits the order of accuracy of the temporal discretization of the FOM. To illustrate this aspect of the methodology, we consider a time-dependent tensor given by:

$$v(x_1, x_2, x_3, t) = \frac{1}{(x_1^b + x_2^b + x_3^b + e^{10t})^{1/b}} \quad x_1, x_2, x_3 \in [1, 200] \quad t \in [0, 1]. \quad (19)$$

The time-dependant tensor  $V(t) \in \mathbb{R}^{200 \times 200 \times 200}$  is obtained by evaluating  $v(x_1, x_2, x_3, t)$  on a uniform grid of  $x_1, x_2, x_3$  at a particular time ( $t$ ). Based on  $V(t)$ , a nonlinear TDE can be obtained as below:

$$\frac{dV}{dt} = -\frac{10 e^{10t}}{b} V^{b+1}. \quad (20)$$

We use explicit second-order and fourth-order Runge-Kutta integrators (RK2 and RK4) for temporal integration of the above TDE. We also considered both Tucker tensor and tensor train low-rank approximation schemes using TT-CUR-DEIM and DEIM-FS algorithms, respectively. We choose  $b = 3$  and final time  $T_f = 1$ . We use the relative error in this example and the rest of the subsequent examples, which is defined as:

$$\mathcal{E}(t) = \frac{\|\hat{V}(t) - V(t)\|_F}{\|V(t)\|_F}.$$

In Figures 3a and 3b, the obtained error at the final time ( $\mathcal{E}(T_f)$ ) is depicted versus time step size ( $\Delta t$ ) for TT-CUR-DEIM and DEIM-FS models. Two fixed-rank values of  $r = 20, 30$  are considered. The figures illustrate that both TT-CUR-DEIM and DEIM-FS methods retain the fourth-order accuracy characteristic of the RK4 scheme, alongside maintaining the second-order accuracy attributed to the RK2 scheme. As anticipated, the TT-CUR-DEIM and DEIM-FS with fourth-order RK scheme saturates to the low-rank error for each  $r$  faster than the second-order RK integration. This confirms the applicability of high-order time integration methods in the proposed TT-CUR-DEIM and DEIM-FS algorithms.

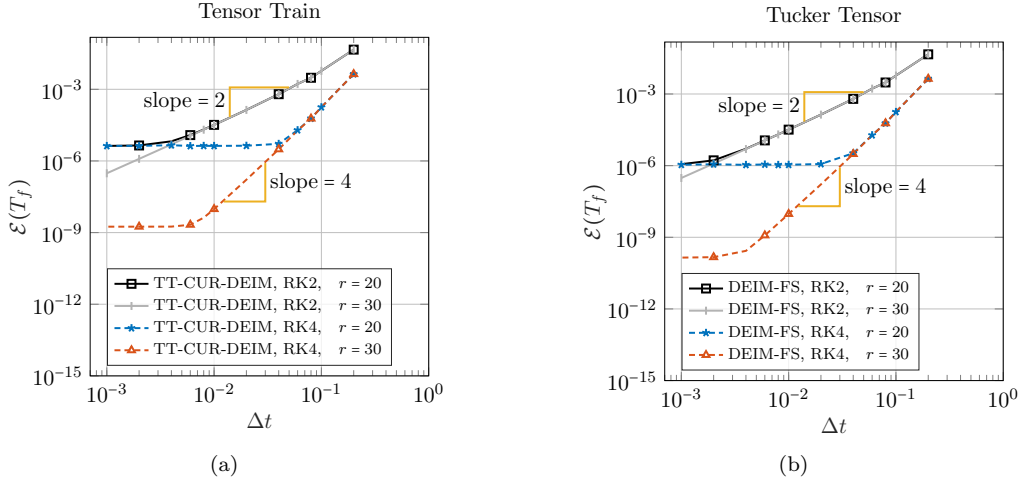


Figure 3: Analytical TDE: Error at the final time ( $\mathcal{E}(T_f)$ ) in solving the given TDE in Eq. (20) versus time step size ( $\Delta t$ ). The second-order and fourth-order Runge-Kutta (RK2 and RK4) are used for time integration with various ranks  $r = 20, r = 30$ . (a) TT-CUR-DEIM; (b) DEIM-FS.

### 3.3. Four-dimensional nonlinear advection-reaction equation

As the third demonstration, we consider a four-dimensional nonlinear advection-reaction given below:

$$\frac{\partial v(\mathbf{x}, t)}{\partial t} = -\mathbf{b} \cdot \nabla v(\mathbf{x}, t) + s(v(\mathbf{x}, t)), \quad \mathbf{x} \in [-5, 5]^4, \quad (21)$$

where  $\mathbf{b} = [-\sin(t), \cos(t), -\sin(\pi+t), \cos(\pi+t)]$  is the advection velocity and  $s(v) = -0.1e^{-v}/(1+v^2)$  is the nonlinear source term. These types of nonlinearity are encountered for example in DLRA of turbulent combustion [47]. The boundary condition is periodic and the initial condition is considered as:

$$v_0(\mathbf{x}) = e^{-(2x_1 - \frac{1}{2})^2} e^{-(2x_2 - \frac{1}{2})^2} e^{-(2x_3 - \frac{1}{2})^2} e^{-(2x_4 - \frac{1}{2})^2}.$$

The presented PDE in Eq. (21) includes non-polynomial nonlinear terms on the right-hand side. In this case,  $\mathcal{F}(\hat{V})$  is a full rank tensor despite  $\hat{V}$  having a low rank. Consequently, the implementation of the standard DLRA requires the explicit formation of the full-dimensional  $\mathcal{F}(\hat{V})$ . The explicit formation of  $\mathcal{F}(\hat{V})$  demands substantial memory allocation and floating-point operations cost that scales at least as  $\mathcal{O}(n^4)$ . The TT-CUR-DEIM algorithm avoids this cost as it never forms the full-rank tensor. Instead, a tensor train approximation of  $\hat{V}^{k-1} + \Delta t \mathcal{F}(t^{k-1}, \hat{V}^{k-1})$  is constructed on the fly.

We employ a spectral-element method for spatial discretization ( $\mathbf{x}$ ), and the fourth-order Runge-Kutta method for temporal integration within time interval  $t \in [0, 4]$ . Each spatial domain is discretized with  $n = n_1 = n_2 = n_3 = n_4 = 81$  points, consisting of 40 elements with a second-order polynomial approximation within each element. The time step is set to  $\Delta t = 1 \times 10^{-3}$ . The TT-CUR-DEIM method is employed for solving the TDE on the low-rank tensor train form. For the error analysis, the relative error with respect to the norm is used. As the analytical solution is unavailable in this TDE, the obtained solution from the FOM is considered the ground truth. To this end, the FOM is solved using  $n = 81$  and  $\Delta t = 1 \times 10^{-3}$ .

We first solve the TDE with the fixed rank  $r = 5$  and  $r = 7$ . Figure 4a indicates that as the rank increases from  $r = 5$  to  $r = 7$ , the error is decreased at all time steps. Then we solve the system with two rank-adaptivity thresholds:  $\epsilon_u = 10^{-4}, 10^{-5}$ . To perform the oversampling process involved in the rank adaptivity, we use GappyPOD+E algorithm with  $m = 5$ . As shown in Figure 4b, a lower value of the upper threshold ( $\epsilon_u$ ) allows more ranks to be involved in solving the system, resulting in a more accurate approximation.

The computational cost of solving the TDE using TT-CUR-DEIM scales linearly with  $n$  and  $d$  despite the non-polynomial nonlinearity of the TDE. In Figure 5a, the computational cost of solving the TDE of Eq. (21) versus  $n$  is shown for the FOM and the TT-CUR-DEIM.

Figure 5b depicts the required memory for storing the RHS of the TT-CUR-DEIM model (i.e. Eq. (12)) relative to the RHS of the FOM (i.e. Eq. (5)). Solving the FOM for this example, requires storing  $n^4 = 43,046,721$  floating point numbers for the RHS of the TDE. While, the RHS of the TT-CUR-DEIM model with  $r = 13$  requires storing  $2nr + 2nr^2 = 29,484$  floating point numbers, resulting in a memory compression ratio of  $43,046,721/29,484 = 1,460$ .

### 3.4. 100-dimensional nonlinear TDE

To demonstrate the capability of the proposed TT-CUR-DEIM method in dealing with high-dimensional tensor differential equations, we consider a 100-dimensional case. The TDE presented in Eq. (23) is obtained from the 100-dimensional time-dependent tensor of Eq. (22).

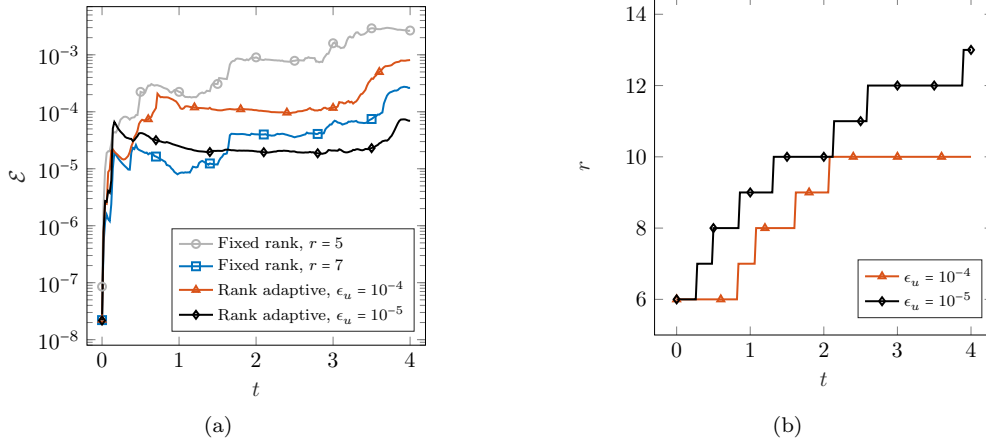


Figure 4: Four-dimensional nonlinear advection equation on low-rank tensor train manifolds: (a) Relative error evolution with fixed rank and adaptive rank; (b) Evolution of  $r$  associated with the rank-adaptive systems plotted in Figure 4a.

$$v(x_1, x_2, \dots, x_{100}, t) = \frac{1}{(x_1^b + x_2^b + \dots + x_{100}^b + e^{10t})^{1/b}} \quad x_1, \dots, x_{100} \in [1, 70] \quad t \in [0, 1], \quad (22)$$

$$\frac{dV}{dt} = -\frac{10 e^{10t}}{b} V^{b+1}. \quad (23)$$

Similar to Example 3.2, the time-dependant tensor  $V(t) \in \mathbb{R}^{70 \times 70 \times \dots \times 70}$  is obtained by evaluating  $v(x_1, \dots, x_{100}, t)$  on a uniform grid of  $x_1, \dots, x_{100}$  at a particular time ( $t$ ). We use explicit fourth-order Runge-Kutta integrators (RK4) for solving the above TDE through the TT-CUR-DEIM. We choose  $b = 0.9$ , which corresponds to a non-polynomial nonlinearity and  $\Delta t = 2 \times 10^{-3}$ . The TDE is solved with two different values of  $\epsilon_l$ . The presented plots in Figure 6a show the relative error over time for  $\epsilon_l = 10^{-7}$  and  $\epsilon_l = 10^{-8}$ . Figure 6b depicts the rank adjustment based on the selected  $\epsilon_l$  for solving the TDE. In case the standard DLRA and FOM are used for solving this TDE, the memory requirements of the RHS of those models scale with  $\mathcal{O}(10^{184})$ . We calculate the error at  $nr^2$  random entries of the solution tensors, where  $n = 70$  and  $r$  is the rank.

#### 4. Conclusion

We present a novel algorithm for the time integration of tensor differential equations on low-rank manifolds. This algorithm is applicable to both tensor train and Tucker tensor low-rank approximations. It advances the low-rank tensor by applying cross approximation algorithms to the time-discrete full-order model. These algorithms, which are based on the Discrete Empirical Interpolation Method (DEIM), sample the time-discrete full-order model at strategically selected entries. For the Tucker tensor low-rank approximation, we utilize DEIM-FS, a method we recently developed [39]. For the tensor train low-rank approximation, we introduce TT-CUR-DEIM, a tensor train cross approximation based on DEIM.

The algorithm offers multiple advantages: (i) Solving nonlinear TDEs on tensor train low-rank manifolds requires evaluating the full-order model at  $\mathcal{O}(r^2 dn)$  entries, which is cost-optimal, i.e.,

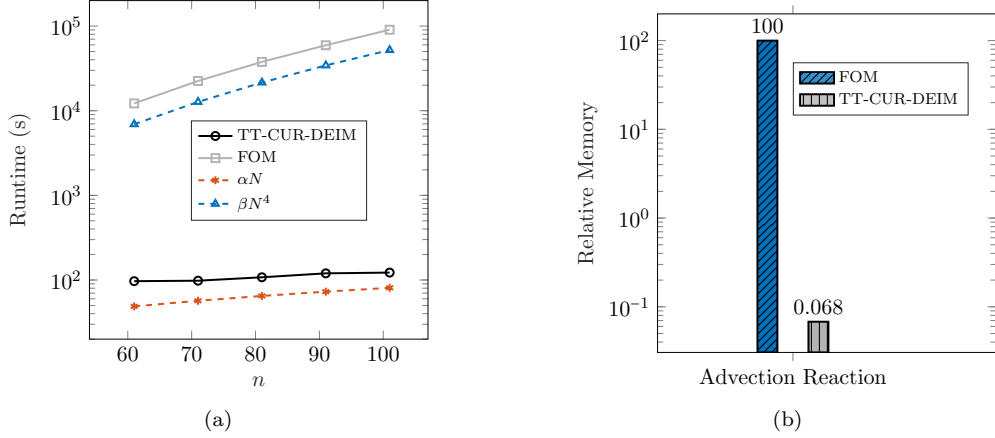


Figure 5: Four-dimensional nonlinear advection equation on low-rank tensor train manifolds: (a) Computational times vs  $n$  (number of discretization points); (b) Comparison of the relative memory requirements for solving the TDE.

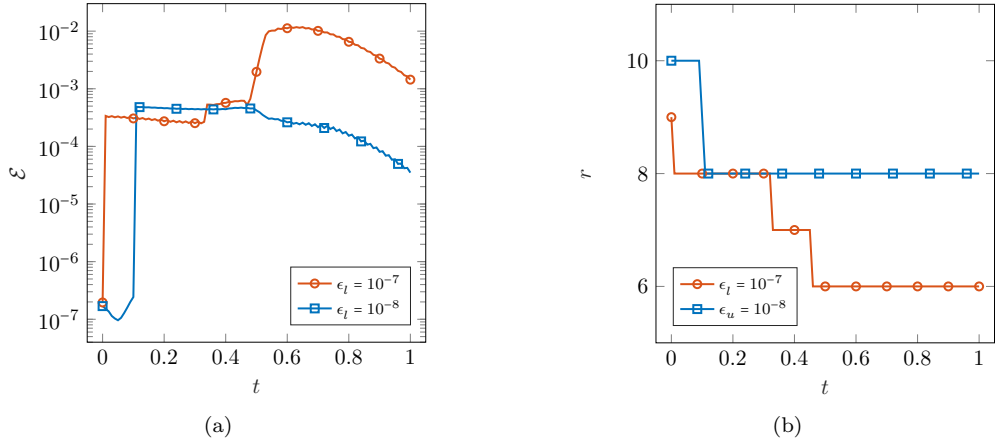


Figure 6: 100-dimensional analytical TDE on low-rank tensor train manifold: (a) Relative error evolution; (b) Evolution of  $r$  associated with systems plotted in Figure 6a.

the minimum number of function evaluation to construct a rank- $r$  tensor train approximation. For a rank- $r$  Tucker tensor decomposition, DEIM-FS requires  $\mathcal{O}(r^d + ndr^{d-1})$  entries, which is significantly smaller than  $n^d$ . The algorithm is agnostic to the type of nonlinearity. (ii) The time-integration scheme does not utilize the inversion of auto-correlation matrices and it is robust in the presence of small or zero singular values. (iii) We demonstrate that the presented algorithm inherits the temporal accuracy of the time-discrete full-order model. In particular, we develop high-order Runge-Kutta time integration schemes. (iii) The algorithm is remarkably simple to implement as it does not utilize tangent space projection and it does require a term-by-term treatment of the right-hand-side terms.

We demonstrate the performance of the algorithm for several test cases including a 100-dimensional nonlinear TDE. The Tucker tensor and tensor train low-rank decomposition demonstrate the potential applicability of the presented algorithm to tensor networks with complex trees.

## Acknowledgments

This work is sponsored by the National Science Foundation (NSF), USA under Grant CBET-2152803 and by the Air Force Office of Scientific Research award no. FA9550-21-1-0247.

## Appendix A. DEIM algorithm

The DEIM pseudocode is presented via Algorithm 2. This algorithm is adopted from [37].

---

<b>Algorithm 2:</b> DEIM Algorithm [37]	
<hr/>	
<b>Input:</b> $\mathbf{U}_p = [\mathbf{u}_1 \quad \mathbf{u}_2 \quad \cdots \quad \mathbf{u}_p]$	
<b>Output:</b> $\mathbf{I}_p$	
1	$[\rho, \mathbf{I}_1] = \max  \mathbf{u}_1 $ <span style="float: right;">▷ choose the first index;</span>
2	$\mathbf{P}_1 = [\mathbf{e}_{\mathbf{I}_1}]$ <span style="float: right;">▷ construct first measurement matrix;</span>
3	<b>for</b> $i = 2$ <b>to</b> $p$ <b>do</b>
4	$\mathbf{P}_i^T \mathbf{U}_i \mathbf{c}_i = \mathbf{P}_i^T \mathbf{u}_{i+1}$ <span style="float: right;">▷ calculate <math>c_i</math>;</span>
5	$\mathbf{R}_{i+1} = \mathbf{u}_{i+1} - \mathbf{U}_i \mathbf{c}_i$ <span style="float: right;">▷ compute residual;</span>
6	$[\rho, \mathbf{I}_i] = \max  \mathbf{R}_{i+1} $ <span style="float: right;">▷ find index of maximum residual;</span>
7	$\mathbf{P}_{i+1} = [\mathbf{P}_i \quad \mathbf{e}_{\mathbf{I}_i}]$ <span style="float: right;">▷ add new column to measurement matrix;</span>
8	<b>end</b>

---

## Appendix B. DEIM for Tucker Tensor Cross approximation

In this appendix, we present the DEIM Tucker cross algorithm that was recently presented in [39]. This algorithm constructs a low-rank Tucker tensor for tensor  $F \in \mathbb{R}^{n_1 \times n_2 \times n_3}$  approximating by sampling  $\mathcal{O}(dr^{d-1}n)$  entries of a tensor with  $n^d$  elements. The algorithm is presented below for convenience.

$$\hat{F} = S_F \times_1 \mathbf{U}_F^{(1)} \times_2 \mathbf{U}_F^{(2)} \times_3 \mathbf{U}_F^{(3)}. \quad (\text{B.1})$$

where  $\hat{F} \in \mathbb{R}^{n_1 \times n_2 \times n_3}$ ,  $S_F \in \mathbb{R}^{r_{F1} \times r_{F2} \times r_{F3}}$ ,  $\mathbf{U}_F^{(1)} \in \mathbb{R}^{n_1 \times r_{F1}}$ ,  $\mathbf{U}_F^{(2)} \in \mathbb{R}^{n_2 \times r_{F2}}$ ,  $\mathbf{U}_F^{(3)} \in \mathbb{R}^{n_3 \times r_{F3}}$ , and  $\mathbf{r}_F = (r_{F1}, r_{F2}, r_{F3})$  is the multi-rank of the Tucker tensor decomposition. The number of selected fibers along the first, second, and third modes are denoted by  $r'_{F1}, r'_{F2}, r'_{F3}$ , respectively.

## Appendix C. DEIM for Tensor Train Cross approximation

Tensor train decomposition can be calculated through a series of singular value decompositions (SVD) [7, Algorithm 1]. However, the SVD-based tensor train decomposition (TT-SVD) requires access to all entries of the given tensor. Storing the high-dimensional tensor entries and computing this sequence of SVDs necessitate substantial memory resources. CUR decompositions can address this issue by constructing low-rank approximations through strategic sampling of the target tensor. The first cross algorithm for the tensor train was presented in [8], where the SVDs are replaced with CURs, and the maximum volume (**maxvol**) algorithm is used for fiber selection [44, 48]. In the

---

**Algorithm 3:** DEIM-FS Tucker tensor low-rank approximation [39]

---

**Input:**

$\tilde{\mathbf{U}}_F^{(i)}$ : matrix of exact or approximate left singular vectors of  $F_{(i)}$ .

$r_{F_i}$ : target Tucker rank.

$F$ : function handle to compute fibers of the target  $F$

**Output:**  $\mathcal{S}_F$ ,  $\mathbf{U}_F^{(1)}$ ,  $\mathbf{U}_F^{(2)}$ ,  $\mathbf{U}_F^{(3)}$

- 1  $\mathbf{p}_i = \text{DEIM}(\tilde{\mathbf{U}}_F^{(i)})$ , ▷ Determine  $\mathbf{p}_1 \in \mathbb{I}^{r'_{F_1}}$ ,  $\mathbf{p}_2 \in \mathbb{I}^{r'_{F_2}}$ ,  $\mathbf{p}_3 \in \mathbb{I}^{r'_{F_3}}$  where  $r'_{F_i} = r_{F_i} + 2$
  - 2  $\mathbf{C}_1 = \left( F(:, \mathbf{p}_2, \mathbf{p}_3) \right)_{(1)}$ , ▷ Calculate  $\mathbf{C}_1 \in \mathbb{R}^{n_1 \times r'_{F_2} r'_{F_3}}$ ,  $\mathbf{C}_2 \in \mathbb{R}^{n_2 \times r'_{F_1} r'_{F_3}}$ ,  $\mathbf{C}_3 \in \mathbb{R}^{n_3 \times r'_{F_1} r'_{F_2}}$   
 $\mathbf{C}_2 = \left( F(\mathbf{p}_1, :, \mathbf{p}_3) \right)_{(2)}$ ,  
 $\mathbf{C}_3 = \left( F(\mathbf{p}_1, \mathbf{p}_2, :) \right)_{(3)}$
  - 3  $[\mathbf{U}_F^{(i)}, \sim, \sim] = \text{SVD}(\mathbf{C}_i, r_{F_i})$  ▷ Calculate the left singular vectors of  $\mathbf{C}_i$  and truncate at rank  $r_{F_i}$
  - 4  $W = F(\mathbf{p}_1, \mathbf{p}_2, \mathbf{p}_3)$  ▷ Form  $\mathcal{W} \in \mathbb{R}^{r'_{F_1} \times r'_{F_2} \times r'_{F_3}}$
  - 5  $\mathcal{S}_F = W \times_1 \mathbf{U}_F^{(1)}(\mathbf{p}_1, :)^{\dagger} \times_2 \mathbf{U}_F^{(2)}(\mathbf{p}_2, :)^{\dagger} \times_3 \mathbf{U}_F^{(3)}(\mathbf{p}_3, :)^{\dagger}$  ▷ Calculate the core tensor ( $\mathcal{S}_F$ )
- 

following, we present a tensor train algorithm based on DEIM. The algorithm largely follows the steps explained in [8]; however, fiber selection is performed with DEIM instead of maxvol. Below, we explain other minor differences between the presented algorithm and the TT-cross algorithm of [8].

Let us consider a tensor  $V(i_1, \dots, i_d)$  of size  $n_1 \times n_2 \times \dots \times n_d$ . In the first step consider the first unfolding of tensor  $V$ , i.e.,  $V_{(1)}$  of size  $n_1 \times n_2 n_3 \dots n_d$ . Assume that a set of  $\mathbf{j}_1$  of indices of  $r_1$  columns of  $V_{(1)}$  are known. In the black-box mode of operation, these indices are initialized randomly and they are updated iteratively until convergence. For solving TDEs, the indices of the previous time step is used without any iteration. The vector  $\mathbf{j}_1$  is a set of  $d - 1$  tuples where each tuple is a multi-index  $(i_2, \dots, i_d)$  that represents a column of  $V_{(1)}$ :

$$\mathbf{j}_1 = [j_l^{(\alpha_1)}], \quad \alpha_1 = 1, \dots, r_1, \quad l = 2, \dots, d,$$

where  $\alpha_1$  corresponds to the column number and  $l$  corresponds to the mode of the tensor. We can represent matrix  $V_{(1)}$  with an interpolatory CUR decomposition as shown below:

$$\hat{V}_{(1)} = \text{CUR}(V_{(1)}) = \mathbf{C}_1 \mathbf{T}_1 \mathbf{R}_1, \quad (\text{C.1})$$

where  $\hat{V}_{(1)}$  is a rank- $r_1$  approximation of  $V_{(1)}$  and  $\mathbf{C}_1 \in \mathbb{R}^{n_1 \times r_1}$  is written as:

$$\mathbf{C}_1(i_1, \alpha_1) = V(i_1, j_2^{(\alpha_1)}, \dots, j_d^{(\alpha_1)}), \quad \alpha_1 = 1, \dots, r_1.$$

Let  $\mathbf{Q}_1$  be obtained via the QR decomposition of  $\mathbf{C}_1$ :  $[\mathbf{Q}_1, \sim] = \text{qr}(\mathbf{C}_1)$ . One approach to calculate a good set of indices along the first mode of  $V$  is to apply the maxvol algorithm to  $\mathbf{Q}_1$  [8, 48]. The corresponding row indices of the submatrix are saved in the set

$$\mathbf{i}_1 = [i_1^{(\alpha_1)}], \quad \alpha_1 = 1, \dots, r_1.$$

As an alternative method for finding the interpolation indices, we propose utilizing DEIM [37]. To this end, we compute the SVD of  $\mathbf{C}_1$ :

$$[\mathbf{U}_1, \sim, \sim] = \text{SVD}(\mathbf{C}_1, r_1).$$

Now we apply DEIM to  $\mathbf{U}_1$  to obtain  $\mathbf{i}_1$ :

$$\mathbf{i}_1 = \text{DEIM}(\mathbf{U}_1).$$

We use the rows of  $V_{(1)}$  at the index  $\mathbf{i}_1$  to interpolate columns of matrix  $V_{(1)}$  onto  $\mathbf{U}_1$ :

$$\hat{V}_{(1)} = \mathbf{U}_1(\mathbf{U}_1(\mathbf{i}_1, :))^{-1} V_{(1)}(\mathbf{i}_1, :) \quad (\text{C.2})$$

Comparing Eqs. (C.2) and (C.1) reveals that:

$$\mathbf{C}_1 \mathbf{T}_1 = \mathbf{U}_1(\mathbf{U}_1(\mathbf{i}_1, :))^{-1} \quad (\text{C.3a})$$

$$\mathbf{R}_1 = V_{(1)}(\mathbf{i}_1, :) \quad (\text{C.3b})$$

The first core tensor is then calculated and stored as:

$$G_1 = \text{reshape}\left(\mathbf{U}_1(\mathbf{U}_1(\mathbf{i}_1, :))^{-1}, [1, n_1, r_1]\right). \quad (\text{C.4})$$

The matrix  $\mathbf{R}_1$  is of size  $r_1 \times n_2 n_3 \dots n_d$  and can be treated as tensor  $R_1$  of dimensionality of  $d-1$  and of size  $r_1 n_2 \times n_3 \times \dots \times n_d$ . Therefore, the size of  $R_1$  scales with  $\mathcal{O}(r_1 n^{d-1})$ , which is very large. However,  $R_1$  is never formed explicitly.

To compute the second core tensor,  $G_2$ , consider the first unfolding of  $R_1$ :

$$R_{1(1)}(\alpha_1 i_2, :) = V_{(1)}(\alpha_1 i_2, :), \quad \alpha_1 = 1, \dots, r_1, \quad i_2 = 1, \dots, n_2, \quad (\text{C.5})$$

where  $R_{1(1)}$  is a matrix of size  $r_1 n_2 \times n_3 \dots n_d$ . Assume that we know a set of  $d-2$  tuples as:

$$\mathbf{j}_2 = [j_l^{(\alpha_2)}], \quad \alpha_2 = 1, \dots, r_2, \quad l = 3, \dots, d. \quad (\text{C.6})$$

Then, we can approximate  $R_{1(1)}$  with a rank- $r_2$  CUR decomposition:

$$\hat{R}_{1(1)} = \text{CUR}(R_{1(1)}) = \mathbf{C}_2 \mathbf{T}_2 \mathbf{R}_2, \quad (\text{C.7})$$

where  $\mathbf{C}_2 \in \mathbb{R}^{r_1 n_2 \times r_2}$  is obtained as:

$$\mathbf{C}_2(\alpha_1 i_2, \alpha_2) = R_1(\alpha_1 i_2, j_3^{(\alpha_2)}, \dots, j_d^{(\alpha_2)}) = V(i_1^{(\alpha_1)}, i_2, j_3^{(\alpha_2)}, \dots, j_d^{(\alpha_2)}). \quad (\text{C.8})$$

Similar to the previous steps, we can compute the left singular vectors of  $\mathbf{C}_2$  as  $[\mathbf{U}_2, \sim, \sim] = \text{SVD}(\mathbf{C}_2, r_2)$ . The indices obtained using the DEIM algorithm are stored in set  $\mathbf{i}_2$ . Since  $\mathbf{i}_2$  is sampled from  $\alpha_1 i_2$  indices, and  $\alpha_1$  corresponds to the indices of  $\mathbf{i}_1$ . Therefore,  $\mathbf{i}_2$  can be expressed as  $\{i_1^{(\alpha_2)}, i_2^{(\alpha_2)}\}$  and moreover they are left-nested as shown below:

$$\{i_1^{(\alpha_2)}\}_{\alpha_2=1}^{r_2} \subset \{i_1^{(\alpha_1)}\}_{\alpha_1=1}^{r_1}. \quad (\text{C.9})$$

The second core tensor is computed as:

$$G_2 = \text{reshape}\left(\mathbf{U}_2(\mathbf{U}_2(\mathbf{i}_2, :))^{-1}, [r_1, n_2, r_2]\right), \quad (\text{C.10})$$

where

$$\mathbf{C}_2 \mathbf{T}_2 = \mathbf{U}_2(\mathbf{U}_2(\mathbf{i}_2, :))^{-1}. \quad (\text{C.11a})$$

$$\mathbf{R}_2 = \hat{R}_{1(1)}(\mathbf{i}_2, :) \quad (\text{C.11b})$$

Using the selected indices  $\mathbf{i}_2$ , the matrix  $\mathbf{R}_2$  of size  $r_2 \times n_3 \dots n_d$  is obtained.

The steps explained above can be similarly repeated to calculate  $G_3, \dots, G_{d-1}$ . Finally,  $G_d$  is obtained as:

$$G_d = V(i_1^{(\alpha_{d-1})}, i_2^{(\alpha_{d-1})}, i_3^{(\alpha_{d-1})}, \dots, :), \quad (\text{C.12})$$

where  $G_d$  is a  $r_{d-1} \times n_d \times 1$  tensor.

We assumed that the right-nested indices  $\mathbf{j}_m$ ,  $m = 1, \dots, d-1$ , are known, while in practice, this is not the case. We follow the same strategy explained in [8], where the  $\mathbf{j}_m$  indices are initialized randomly. By following the above steps, a tensor train approximation of  $V$  is obtained, and the left-nested index sets  $\mathbf{i}_m$ ,  $m = 1, \dots, d-1$ , are calculated using the DEIM algorithm. Then, a reverse iteration is performed by peeling off the modes of the target tensor in reverse order (i.e.,  $d, d-1, \dots, 1$ ), i.e., from right to left. In the reverse iteration, the calculated  $\mathbf{i}_m$  indices from the forward iteration are used to determine the new index sets  $\mathbf{j}_m$ , and these reverse-forward iterations are repeated until convergence.

In this paper, if DEIM is utilized for nested index selection, the TT-cross algorithm is referred to as TT-CUR-DEIM, and the cross algorithm presented in [8] is referred to as TT-CROSS-maxvol.

#### Appendix D. Cross Algorithm for the Time Integration of Tensor Train Low-Rank Approximation

In this section, we present an algorithm for performing the explicit time integration of TDEs on low-rank manifold using TT-CUR-DEIM. The algorithm computes the solution at the time step  $k$  ( $\hat{V}^k$ ), in low-rank tensor train form given the state of the previous time step tensor ( $\hat{V}^{k-1}$ ) in the tensor train form. We explain the algorithm for a three-dimensional tensor for simplicity ( $d = 3$ ). The steps of the algorithm are explained below:

1. **Computing  $V_1^k$ :**  $V_1^k$  is a tensor of size  $1 \times n_1 \times r_1$  and can be reshaped into a matrix of size  $n_1 \times r_1$ . The sets  $[j_2^{(\alpha_1)}]$  and  $[j_3^{(\alpha_1)}]$  are the left-nested index sets obtained at the previous time step and are being used as the right-nested indices at the current time step. Computing  $V_1^k$  is equivalent to computing  $\mathbf{C}_1$  in TT-CUR-DEIM. In other words,  $V_1^k$  represents  $\mathbf{C}$  in the CUR decomposition of  $V_{(1)}^k$  (the unfolded  $V^k$  along the first mode). According to Eq. (8),  $V_1^k(1, :, \alpha_1) = \hat{V}_1^{k-1}(1, :, \alpha_1) + \Delta t \overline{\mathcal{F}}(\hat{V}_1^{k-1}(1, :, \alpha_1))$ , where  $\alpha_1$  runs from 1 to  $r_1$ . For the TDEs obtained from discretizing a PDE, the function  $F(\sim)$  involves discrete differential operators. Since the derivative calculation requires adjacent points of the DEIM-selected indices, the adjacent indices must be determined for the calculation of  $V_1^k$ . This process depends on the numerical scheme employed for spatial discretization. For instance, in the spectral element method, calculating the derivative at a given spatial point requires accessing the values of neighboring points within the same element [25]. We use the subscript "a" to denote the additional fiber indices (e.g.,  $j_{a2}^{(\alpha_1)}$  denotes the adjacent points of  $j_2^{(\alpha_1)}$ ).
2. **Computing  $G_1^k$ :** In order to compute  $G_1^k \in \mathbb{R}^{1 \times n_1 \times r_1}$ , we first need to calculate the left singular vectors of  $V_1^k$ . This is done to avoid ill-conditioning issues by computing orthonormal bases of the columns space of  $V_1^k$  (as mentioned  $V_1^k$  can also be treated as a  $n_1 \times r_1$  matrix). Therefore, we compute SVD of  $V_1^k$  and truncate it at rank- $r_1$  ( $[\mathbf{U}_1, \sim, \sim] = \text{SVD}(V_1^k, r_1)$ ). Once  $\mathbf{U}_1 \in \mathbb{R}^{n_1 \times r_1}$  is calculated, DEIM is utilized to determine the first set of left-nested indices

- ( $\mathbf{i}_1 = \text{DEIM}(\mathbf{U}_1)$ ). The set  $\mathbf{i}_1 \in \mathbb{I}^{r_1}$  actually contains  $r_1$  indices presented as  $\mathbf{i}_1 = [i_1^{(\alpha_1)}]$ ,  $\alpha_1 = 1, \dots, r_1$ . Finally, the first tensor train core tensor is computed as  $G_1^k = \mathbf{U}_1 (\mathbf{U}_1(\mathbf{i}_1, :))^{-1}$ .
3. **Computing  $V_2^k$ :** which is a tensor of size  $r_1 \times n_2 \times r_2$ . To compute  $V_2^k$ , we use the left-nested indices ( $[i_1^{(\alpha_1)}]$ ) calculated in (2) and right-nested indices obtained in the previous time step. This step is equivalent to computing  $\mathbf{C}_2$  in TT-CUR-DEIM algorithm presented in Eq.(C.8). We compute  $V_2^k$  as  $V_2^k(\alpha_1, :, \alpha_2) = \hat{V}_2^{k-1}(\alpha_1, :, \alpha_2) + \Delta t \mathcal{F}(t^{k-1}, \hat{V}_2^{k-1}(\alpha_1, :, \alpha_2))$ , where  $\alpha_1 = 1, \dots, r_1$  and  $\alpha_2 = 1, \dots, r_2$ . Similar to (1), the adjacent points of  $i_1^{(\alpha_1)}$  and  $j_3^{(\alpha_2)}$  may required for calculation of the derivatives.
  4. **Computing  $G_2^k$ :** To compute  $G_2^k \in \mathbb{R}^{r_1 \times n_2 \times r_2}$ , we first reshape  $V_2^k \in \mathbb{R}^{r_1 \times n_2 \times r_2}$  to a matrix of size  $r_1 n_2 \times r_2$ . We use MATLAB notation for this operation as `reshape( $V_2^k$ ,  $[r_1 n_2, r_2]$ )`. Then, we need to calculate the left singular vectors of the obtained matrix using SVD and truncate it at rank  $r_2$  as  $[\mathbf{U}_2, \sim, \sim] = \text{SVD}(\text{reshape}(V_2^k, [r_1 n_2, r_2]), r_2)$ . Subsequently,  $\mathbf{U}_2 \in \mathbb{R}^{r_1 n_2 \times r_2}$  is used to determine the second set of DEIM-selected left-nested indices ( $\mathbf{i}_2 = \text{DEIM}(\mathbf{U}_2)$ ). As mentioned in Appendix C,  $\mathbf{i}_2 \in \mathbb{I}^{r_2}$  is sampled from  $r_1 n_2$  indices, and  $r_1$  corresponds to the indices of  $\mathbf{i}_1$  determined in (2), therefore,  $\mathbf{i}_2$  can be separated as indices of the form  $\{[i_1^{(\alpha_2)}], [i_2^{(\alpha_2)}]\}$ ,  $\alpha_2 = 1, \dots, r_2$ . Accordingly, the second tensor train core tensor is calculated as  $G_2^k = \text{reshape}(\mathbf{U}_2(\mathbf{U}_2(\mathbf{i}_2, :))^{-1}, [r_1, n_2, r_2])$ .
  5. **Computing  $V_3^k$  and  $G_3^k$ :** As mentioned in Section Appendix C, the third tensor train core tensor ( $G_3^k \in \mathbb{R}^{r_2 \times n_3 \times 1}$ ) is equal to  $V_3^k$ . Calculation of  $G_3^k$  corresponds to the Eq. (C.12) presented in TT-CUR-DEIM algorithm. The left-nested indices ( $[i_1^{(\alpha_2)}]$  and  $[i_2^{(\alpha_2)}]$ ) obtained in (4) and their adjacent points are used to compute  $V_3^k$  as  $V_3^k(\alpha_2, :, 1) = \hat{V}_3^{k-1}(\alpha_2, :, 1) + \Delta t F(\hat{V}_3^{k-1}(\alpha_2, :, 1))$ , where  $\alpha_2 = 1, \dots, r_2$ .
  6. **Setting the stage for the next time step:** Based on TT-CUR-DEIM algorithm, the reverse-forward iterations are needed for convergence of the left and right-nested index sets. And the reverse iteration is performed by separating the tensor modes in the reverse order (i.e.  $d, d-1, \dots, 1$ ). In the proposed tensor train time integration cross algorithm, we skip this iterative process by taking advantage of the DEIM-selected indices from the previous time step. However, in order to use those indices in the current time step, we need to separate the tensor modes in the reverse order. In algorithmic language, this reverse mode separation can be done by flipping the axes of the obtained  $G_0^k, G_1^k, G_2^k$  in the current time step and using them in the next time step as  $G_2^{k-1}, G_1^{k-1}, G_0^{k-1}$ , respectively. Subsequently, we assign  $[j_2^{(\alpha_1)}] = [i_2^{(\alpha_2)}]$ ;  $[j_3^{(\alpha_1)}] = [i_1^{(\alpha_2)}]$ ;  $[j_3^{(\alpha_2)}] = [i_1^{(\alpha_1)}]$ .

## References

- [1] M. Donello, G. Palkar, M. H. Naderi, D. C. Del Rey Fernández, and H. Babaei, "Oblique projection for scalable rank-adaptive reduced-order modelling of nonlinear stochastic partial differential equations with time-dependent bases," *Proceedings of the Royal Society A: Mathematical, Physical and Engineering Sciences*, vol. 479, no. 2278, p. 20230320, 2023.
- [2] T. G. Kolda and B. W. Bader, "Tensor decompositions and applications," *SIAM Review*, vol. 51, no. 3, pp. 455–500, 2009.
- [3] L. Grasedyck, D. Kressner, and C. Tobler, "A literature survey of low-rank tensor approximation techniques," *GAMM-Mitteilungen*, vol. 36, pp. 53–78, 2020/07/06 2013.
- [4] L. R. Tucker, "Some mathematical notes on three-mode factor analysis," vol. 31, no. 3, pp. 279–311, 1966.

- [5] R. A. Harshman, "Foundations of the PARAFAC procedure: Models and conditions for an "explanatory" multi-modal factor analysis," *UCLA Working Papers in Phonetics*, vol. 16, pp. 1–84, 1970.
- [6] L. Grasedyck, "Hierarchical singular value decomposition of tensors," *SIAM Journal on Matrix Analysis and Applications*, vol. 31, pp. 2029–2054, 2023/12/11 2010.
- [7] I. V. Oseledets, "Tensor-train decomposition," *SIAM Journal on Scientific Computing*, vol. 33, pp. 2295–2317, 2020/03/23 2011.
- [8] I. Oseledets and E. Tyrtysnikov, "TT-cross approximation for multidimensional arrays," *Linear Algebra and its Applications*, vol. 432, no. 1, pp. 70–88, 2010.
- [9] L. Li, W. Yu, and K. Batselier, "Faster tensor train decomposition for sparse data," *Journal of Computational and Applied Mathematics*, vol. 405, p. 113972, 2022.
- [10] K. Batselier, Z. Chen, and N. Wong, "Tensor network alternating linear scheme for MIMO volterra system identification," *Automatica*, vol. 84, pp. 26–35, 2017.
- [11] Z. Zhang, X. Yang, I. V. Oseledets, G. E. Karniadakis, and L. Daniel, "Enabling high-dimensional hierarchical uncertainty quantification by ANOVA and tensor-train decomposition," *IEEE Transactions on Computer-Aided Design of Integrated Circuits and Systems*, vol. 34, no. 1, pp. 63–76, 2015.
- [12] D. Kressner and A. Uschmajew, "On low-rank approximability of solutions to high-dimensional operator equations and eigenvalue problems," *Linear Algebra and its Applications*, vol. 493, pp. 556–572, 2016.
- [13] Z. Chen, K. Batselier, J. A. K. Suykens, and N. Wong, "Parallelized tensor train learning of polynomial classifiers," *IEEE Transactions on Neural Networks and Learning Systems*, vol. 29, no. 10, pp. 4621–4632, 2018.
- [14] Y. Wang, W. Zhang, Z. Yu, Z. Gu, H. Liu, Z. Cai, C. Wang, and S. Gao, "Support vector machine based on low-rank tensor train decomposition for big data applications," in *2017 12th IEEE Conference on Industrial Electronics and Applications (ICIEA)*, pp. 850–853, 2017.
- [15] W. Wang, V. Aggarwal, and S. Aeron, "Tensor train neighborhood preserving embedding," *IEEE Transactions on Signal Processing*, vol. 66, no. 10, pp. 2724–2732, 2018.
- [16] A. Cichocki, "Era of big data processing: A new approach via tensor networks and tensor decompositions," 2014.
- [17] O. Koch and C. Lubich, "Dynamical tensor approximation," *SIAM Journal on Matrix Analysis and Applications*, vol. 31, pp. 2360–2375, 2017/04/02 2010.
- [18] C. Lubich, B. Vandereycken, and H. Walach, "Time integration of rank-constrained Tucker tensors," *SIAM Journal on Numerical Analysis*, vol. 56, no. 3, pp. 1273–1290, 2018.
- [19] A. Veit and L. R. Scott, "Using the tensor-train approach to solve the ground-state eigenproblem for hydrogen molecules," *SIAM Journal on Scientific Computing*, vol. 39, no. 1, pp. B190–B220, 2017.
- [20] S. Dolgov, D. Kalise, and K. K. Kunisch, "Tensor decomposition methods for high-dimensional Hamilton-Jacobi-Bellman equations," *SIAM Journal on Scientific Computing*, vol. 43, no. 3, pp. A1625–A1650, 2021.
- [21] N. Gourianov, M. Lubasch, S. Dolgov, Q. Y. van den Berg, H. Babaei, P. Givi, M. Kiffner, and D. Jaksch, "A quantum-inspired approach to exploit turbulence structures," *Nature Computational Science*, vol. 2, no. 1, pp. 30–37, 2022.
- [22] I. Gavriluk and B. N. Khoromskij, "Tensor numerical methods: Actual theory and recent applications," *Computational Methods in Applied Mathematics*, vol. 19, no. 1, pp. 1–4, 2019.
- [23] M. Donello, M. H. Carpenter, and H. Babaei, "Computing sensitivities in evolutionary systems: A real-time reduced order modeling strategy," *SIAM Journal on Scientific Computing*, pp. A128–A149, 2022/01/19 2022.
- [24] A. Amiri-Margavi and H. Babaei, "Low-rank solution operator for forced linearized dynamics with unsteady base flows," 2023.
- [25] M. H. Naderi and H. Babaei, "Adaptive sparse interpolation for accelerating nonlinear stochastic reduced-order modeling with time-dependent bases," *Computer Methods in Applied Mechanics and Engineering*, vol. 405, p. 115813, 2023.
- [26] C. Lubich, I. V. Oseledets, and B. Vandereycken, "Time integration of tensor trains," *SIAM Journal on Numerical Analysis*, vol. 53, no. 2, pp. 917–941, 2015.
- [27] J. Haegeman, C. Lubich, I. Oseledets, B. Vandereycken, and F. Verstraete, "Unifying time evolution and optimization with matrix product states," *Phys. Rev. B*, vol. 94, p. 165116, 2016.
- [28] G. Ceruti and C. Lubich, "An unconventional robust integrator for dynamical low-rank approximation," *BIT Numerical Mathematics*, vol. 62, no. 1, pp. 23–44, 2022.
- [29] C. Lubich and I. V. Oseledets, "A projector-splitting integrator for dynamical low-rank approximation," *BIT Numerical Mathematics*, vol. 54, no. 1, pp. 171–188, 2014.
- [30] E. Kieri, C. Lubich, and H. Walach, "Discretized dynamical low-rank approximation in the presence of small singular values," *SIAM Journal on Numerical Analysis*, vol. 54, no. 2, pp. 1020–1038, 2016.

- [31] G. Ceruti, J. Kusch, and C. Lubich, “A rank-adaptive robust integrator for dynamical low-rank approximation,” *BIT Numerical Mathematics*, vol. 62, no. 4, pp. 1149–1174, 2022.
- [32] G. Ceruti, C. Lubich, and D. Sulz, “Rank-adaptive time integration of tree tensor networks,” *SIAM Journal on Numerical Analysis*, vol. 61, no. 1, pp. 194–222, 2023.
- [33] G. Ceruti, C. Lubich, and H. Walach, “Time integration of tree tensor networks,” *SIAM Journal on Numerical Analysis*, vol. 59, no. 1, pp. 289–313, 2021.
- [34] G. Ceruti, L. Einkemmer, J. Kusch, and C. Lubich, “A robust second-order low-rank BUG integrator based on the midpoint rule,” 2024.
- [35] E. Kieri and B. Vandereycken, “Projection methods for dynamical low-rank approximation of high-dimensional problems,” *Computational Methods in Applied Mathematics*, vol. 19, no. 1, pp. 73–92, 2019.
- [36] A. Rodgers, A. Dektor, and D. Venturi, “Adaptive integration of nonlinear evolution equations on tensor manifolds,” *Journal of Scientific Computing*, vol. 92, no. 2, p. 39, 2022.
- [37] S. Chaturantabut and D. C. Sorensen, “Nonlinear model reduction via discrete empirical interpolation,” *SIAM Journal on Scientific Computing*, vol. 32, no. 5, pp. 2737–2764, 2010.
- [38] C. Pagliantini and F. Vismara, “Fully adaptive structure-preserving hyper-reduction of parametric hamiltonian systems,” 2023.
- [39] B. Ghahremani and H. Babaei, “A DEIM Tucker tensor cross algorithm and its application to dynamical low-rank approximation,” *Computer Methods in Applied Mechanics and Engineering*, vol. 423, p. 116879, 2024.
- [40] A. Dektor, “A collocation method for nonlinear tensor differential equations on low-rank manifolds,” 2024.
- [41] C. Lubich, T. Rohwedder, R. Schneider, and B. Vandereycken, “Dynamical approximation by hierarchical Tucker and tensor-train tensors,” *SIAM Journal on Matrix Analysis and Applications*, vol. 34, no. 2, pp. 470–494, 2013.
- [42] A. Rodgers, A. Dektor, and D. Venturi, “Adaptive integration of nonlinear evolution equations on tensor manifolds,” *Journal of Scientific Computing*, vol. 92, no. 2, p. 39, 2022.
- [43] S. Dolgov, D. Kressner, and C. Strössner, “Functional Tucker approximation using Chebyshev interpolation,” *SIAM Journal on Scientific Computing*, vol. 43, no. 3, pp. A2190–A2210, 2021.
- [44] S. A. Goreinov, E. E. Tyrtyshnikov, and N. L. Zamarashkin, “A theory of pseudoskeleton approximations,” *Linear Algebra and its Applications*, vol. 261, no. 1, pp. 1–21, 1997.
- [45] B. Peherstorfer, Z. Drmač, and S. Gugercin, “Stability of discrete empirical interpolation and gappy proper orthogonal decomposition with randomized and deterministic sampling points,” *SIAM Journal on Scientific Computing*, vol. 42, no. 5, pp. A2837–A2864, 2020.
- [46] M. W. Mahoney and P. Drineas, “CUR matrix decompositions for improved data analysis,” *Proceedings of the National Academy of Sciences*, vol. 106, no. 3, pp. 697–702, 2009.
- [47] D. Ramezani, A. G. Nouri, and H. Babaei, “On-the-fly reduced order modeling of passive and reactive species via time-dependent manifolds,” *Computer Methods in Applied Mechanics and Engineering*, vol. 382, p. 113882, 2021.
- [48] S. A. Goreinov, I. V. Oseledets, D. V. Savostyanov, E. E. Tyrtyshnikov, and N. L. Zamarashkin, *How to Find a Good Submatrix*, pp. 247–256.